Arabian Journal for Science and Engineering
https://doi.org/10.1007/s13369-022-06925-z

RESEARCH ARTICLE-MECHANICAL ENGINEERING

# Neuro-Computing for Hall Current and MHD Effects on the Flow of Micro-Polar Nano-Fluid Between Two Parallel Rotating Plates

**Hakeem Ullah[1] · Muhammad Shoaib[2] · Ajed Akbar[1] · Muhammad Asif Zahoor Raja[3] · Saeed Islam[1] · Kottakkaran Sooppy Nisar[4]**

Received: 6 December 2021 / Accepted: 21 April 2022


**Abstract**

The present works focus on the effects of electric and magnetic fields on the flow of micro-polar nano-fluid between two parallel plates with rotation under the impact of Hall current (EMMN-PPRH) has considered by using Artificial Neural Networks with the scheme of Levenberg–Marquardt backpropagation (ANN-SLMB). The nonlinear PDEs are transformed into nonlinear ODEs by employing similarity variables. By varying different parameters such as coupling parameter, electric parameter, rotation parameter, viscosity parameter, Prandtl number and the Brownian motion parameter, a dataset for recommended ANN-SLMB is produced for numerous scenarios through utilizing homotopy analysis method (HAM). The ANN-SLMB training, testing and validation technique have been used to analyze the approximate solution of individual cases, and the recommended model has matched for confirmation. After that, regression analysis, MSE, and histogram investigations were utilized to validate the proposed ANN-SLMB. The recommended technique is distinguished nearest of the suggested and reference findings, with an accuracy level ranging from $10^{-09}$ to $10^{-11}$.

**Keywords** Nano-fluid · HAM · Levenberg–Marquardt Scheme · Artificial neural network

✉ Hakeem Ullah
hakeemullah1@gmail.com

✉ Muhammad Asif Zahoor Raja
rajamaz@yuntech.edu.tw

✉ Kottakkaran Sooppy Nisar
n.sooppy@psau.edu.sa

Muhammad Shoaib
dr.shoaib@cuiatk.edu.pk

Ajed Akbar
ajedakbar@gmail.com

Saeed Islam
saeedislam@awkum.edu.pk

[1] Department of Mathematics, Abdul Wali Khan University, Mardan 23200, Khyber Pakhtunkhwa, Pakistan

[2] Department of Mathematics, COMSATS University Islamabad, Attock Campus, Attock 43600, Pakistan

[3] Future Technology Research Center, National Yunlin University of Science and Technology, 123 University Road, Section. 3, Douliou, Yunlin 64002, Taiwan, R.O.C.

[4] Department of Mathematics, College of Arts and Sciences, Prince Sattam Bin Abdulaziz University, Wadi Aldawaser, Saudi Arabia

## List of Symbols

| | |
|---|---|
| $\overline{B}$ | Magnetic field |
| $C$ | Fluid concentration |
| $D_B$ | Brownian diffusion of nano-fluids |
| $\overline{E}$ | Electric field intensity |
| $c_p$ | Specific heat |
| $D_T$ | Thermophoretic diffusion of nano-fluids |
| $C_f$ | Skin friction coefficient |
| $h$ | Distance between the plates |
| $J_w$ | Mass flux |
| $\overline{J}$ | Current density |
| $Kr$ | Rotation parameter |
| $m$ | Hall parameter |
| $M$ | Magnetic parameter |
| $\overline{N}$ | Micro-rotation angular velocity |
| $k$ | The boundary parameter |
| $n_e$ | Number density of electron |
| $N_1$ | Coupling parameter |
| $Nb$ | Brownian motion |
| $O(0, 0, 0)$ | Origin |
| $N_2$ | Spin gradient viscosity parameter |
| $Nt$ | Thermophoretic parameter |

Published online: 24 May 2022

| | |
|---|---|
| $Nu$ | Nusselt number |
| $N_3$ | Micro-polar fluid constant |
| Pr | Prandtl number |
| $Q_w$ | Heat flux |
| Re | Viscosity parameter |
| $EI$ | Electric parameter |
| ANN | Artificial Neural Network |
| SLMB | Scheme Levenberg–Marquardt backpropagation |
| AE | Absolute error |
| $f$,$g$ | Velocity distributions |
| $G$ | Micro-rotation profile |
| $\mathrm{Re}_x$ | Local Reynolds number |
| $\overline{S}_{xy}$ | Cauchy stress tensor |
| $Sc$ | Schmidt number |
| $Sh$ | Sherwood number |
| $t_e$ | Times of electron Collision |
| $T$ | Fluid temperature |
| $(\overline{u}, \overline{v}, \overline{w})$ | Velocities components |
| $\overline{v}_0$ | Suction/Injection velocity |
| $e$ | Charge of electron |
| $(x, y, z)$ | Coordinates |
| $P_e$ | Pressure of electron |
| Greek | Letters |
| $\rho_f$ | Base fluid density |
| $\delta$ | Transpiration parameter |
| $v$ | Kinematic coefficient of viscosity |
| $\widehat{\kappa}$ | Vertex viscosity |
| $\eta$ | Similarity variable |
| $\mu$ | Dynamic viscosity |
| $\Omega$ | Angular velocity |
| $\tau^*$ | Nano-particles and heat capacity ratio |
| $\omega_e$ | Electron Oscillating frequency |
| $\Theta$ | Dimensional temperature profile |
| $\Phi$ | Dimensional concentration profile |
| $\alpha$ | Stretching parameter |
| $\alpha^*$ | Thermal diffusivity |
| $\sigma_{nf}$ | Electrical conductivity |

## 1 Introduction

Artificial neural networks (ANNs) are interesting and significant paradigms associated with artificial intelligence (AI). ANNs can evolve in a variety of ways, depending on the data that feeds through the network throughout the learning process, whether externally or internally. To increase the performance of a multilayer perceptron (MLP) network, an artificial neural network uses the backpropagation (BP) technique to undertake simultaneous training. It is the most widely used, effective, and easy-to-learn paradigm for complex multi-layered networks. The Levenberg–Marquardt methodology/algorithm (LMA) is a ground-breaking, convergent, reliable technique for artificial neural networks (ANNs) that provides a numerical solution to a wide range of fluid flow problems. Dreyfus employed backpropagation in 1973 to modify controller settings in proportion to error gradients. Werbos' (1975) backpropagation technique made multi-layer network training practicable. In 1982, he popularized Linnainmaa's AD approach by applying it to neural networks [1, 2]. Backpropagation has been widely used as a learning mechanism in feed-forward multilayer neural networks.

Certain researchers have recently used this technique to explore mass and heat transport aspects, as well as non-Newtonian fluid flow systems. Ahmad et al. [3] looked at intelligent computing approaches for analyzing nonlinear reactive fluid transport models in soft-tissues and microvessels. Shoaib et al. [4] used neural networks to explore the generation of entropy under the influence of MHD and thermal radiation. Sabir et al. [5] used a computational intelligence approach using Levenberg–Marquardt backpropagation neural networks to describe the fourth-order nonlinear system of the Emden–Fowler model. Uddin et al. [6] showed how to integrate magnetic and radiation impacts to comprehend the research of a Maxwell Nano-liquid thin film stream over a stretchable and spinning disk using LM-NN-based computational intelligence. Khan et al. [7] used a BNN-LMS to investigate heat transport between two permeable parallel plates of steady Nano-fluids applying Thermophoresis and Brownian impacts. Shah et al. [8] propose using neural networks to investigate the design of neural network-based intelligent calculation for the numerical behavior of unsteady 3D flow in the Powell–Eyring magneto-nanofluidic model.

The study of the magnetic characteristics and performance of electrically conducting fluids is known as magnetohydrodynamics (MHD). Magnetofluids include electrolytes, plasmas, saltwater, and liquid metals. The Magnetohydrodynamics field was initially described by Hannes Alfven [9]. Magnetohydrodynamics has a wide range of applications in engineering and technology, including crystal growth, plasma, electromagnetic casting, liquid–metal cooling of reactors, MHD sensors, magnetic drug targeting, and MHD power production. Magnetohydrodynamics is affected by the intensity of magnetic generations. Whenever the magnetic force increases, the Hall Effect caused by the Hall current cannot be ignored. Edwin Hall [10] is the forerunner to introduce the idea of Hall current. It is important and intriguing to study hydrodynamic issues. The effect of Hall currents improves hydrodynamical problems. Ahmed and Zueco [11] used the Hall effects to study the heat and mass transfer with a rotating and porous medium and found an accurate solution to the simulated problem. Pop and Soundalgekar [12] investigated the Hall effect in the time-dependent

magnetohydrodynamic viscous flowing fluid. Sulochana [13] examined unsteady flow across a porous material in a rotating parallel plate, while taking Hall effects into consideration. Awais et al. [14] studied the effect of viscous dissipation on convection Jeffery fluid flow under the impacts of ion slip and Hall current. Abdel Aziz [15] explored the Hal effects on viscid and nano-fluid flow, as well as heat transfer via a stretched sheet.

Micro-polar fluids are such types of fluids that have a micro-structure and an irregular stress tensor. Eringen [16, 17] was the first one to propose the concept of micro-polar fluid. Lukaszewicz [18] discusses detailed research and a wider variety of applications for micro-polar fluids. Physically, micro-polar fluids are defined as fluids with irregularly orientated liquids floating in a viscous channel. All such fluids are utilized in the study of blood, colloidal suspensions flow, exotic emollients, liquefied crystals, brain fluid, paints, and turbulent shear flows. Mohammeadein and Gorla [19] performed the first research of micro-polar fluids on a horizontal plate of mass dissemination under the effect of an oblique magnetic field. Kasivishwanathan et al. [20] studied the flow of magnetohydrodynamics micro-polar fluid and accomplished a set of accurate solutions. Bhargava et al. [21] explored the mixed convection flow micro-polar fluid flow through a permeable stretched sheet using a finite element solution. Agarwal and Dhanapal [22] investigated the flows of micro-polar fluid with free convection between two parallel permeability upright plates using numerical solutions. Srinivasacharya et al. [23] studied the unsteady stokes micro-polar fluid between permeable and parallel plates. Ziabakhsh et al. [24] used a homotopic approach to solve the problem of micro-polar nano-fluid in a permeable surface through the influence of heat and mass transmission. Nazar et al. [25] and Ishak et al. [26] considered the stagnation point flow of micro-polar fluid across a strained surface. Nadeem et al. [27, 28] examined the micro-polar nano-fluid in two parallel and horizontal rotating plates. The problem's analytical solution had been determined, and the included parameters had been investigated in their research.

For the unusual aspects of nano-liquids that make them efficient in a variety of applications, nano-fluids are exploited in medicinal processes, hybrid-powered engines, fuel cells, and micro-electronics, now these are primarily utilized in nanotechnologies fields [29]. Wang et al. [30] provided a quick overview of nano-fluids based on their research and application areas. The flow of nano-fluid across parallel plates is a frequent and traditional problem in several applications in the petroleum industry, crude oil purification, accelerators, aerodynamic heating, MHD power generators and pumps, the design of liquid metal cooling systems, and various vehicle sprays. Goodman [31] was the pioneer to use parallel plates to analyze viscous fluids. Sheikholeslami et al. [32, 33] used magnetohydrodynamics (MHD) effects to explore the flow of nano-fluid of viscous fluids in three dimensions across rotating parallel plates. Attia et al. [34] investigated magnetohydrodynamically influenced viscous flows across parallel plates. Borkakoti and Bharali [35] studied magnetohydrodynamics viscous flows between parallel plates with a stretched sheet as one of the plates. They utilized numerical approaches to solve the simulated problems and detailed descriptions of the impacts of various parameters. Sheikholeslami's current work on nano-fluids and their applications with various performance, characteristics, and impacts using various numerical and analytical approaches may be found in [36–39]. Rokni et al. [40] and Tauseef et al. [41] deliberated the impacts of magnetohydrodynamics and temperature on nano-fluid flow on rotating parallel plates. Mahmoodi and Kandelousi [42] utilized the differential transformation technique to study the hydromagnetic influence of Kerosene-Alumina nano-fluid flow in the occurrence of heat transfer analysis.

The flow of fluid in a rotating system is a naturally occurring phenomenon. Such rotation takes place throughout the fluid particles and increases as the fluid starts to flow. As a result, rotations play a role in natural fluid flow phenomena. Greenspan [43] explored in-depth the topic of the flow of fluid in a system of rotation. Geoffrey and Taylor [44] introduced the experimental notion of the motion of viscous fluid in a system of rotation. Vajravelua and Kumar [45] looked at the flow of magnetohydrodynamics viscous fluid between two rotating parallel and horizontal plates, one of which was stretched and the other porous. They have developed a numerical solution and examined the effects of various physical factors. Mehmood and Asif [46] extended their work. Hayat et al. [47, 48] extended their study into two and three dimensions by using several models to study the flow of non-Newtonian fluid with rotation.

Nano-fluids have enhanced thermophysical characteristics and might be used as heat transfer fluids. In general, such fluids are made up of nanometer-sized particles known as nanoparticles. Such fluids are colloidal suspensions of nanoparticles in a base fluid that are being manufactured. Nanoparticles are utilized in nano-fluids that include metals, carbides, oxides, or carbon nanotubes. Choi [49] praised the fact that thermal conductivity and convective heat transfer of nanoparticles are significantly increased proportionally to heat transmission. The heat flow process is increased, which improves heat transmission. Many researchers and scientists from all around the world were drawn to the nano-fluids topic. These fluids are used in a variety of technical and industrial applications, such as high-power lasers, cooling nuclear systems, solar water heating, microwave tubes, biomedical applications and engine transmission oil [50].

The homotopy analysis method has been used to solve an increasing number of nonlinear ordinary/partial differential equations in science, economics, and engineering during

the last two decades. [51] For example, the wave resonance criteria of an arbitrary number of travelling gravity waves were used to find numerous steady-state resonant waves in deep and finite water depth [52], which corresponded with Phillips' criterion for four waves of modest amplitude. Debnath and Das [53] use an artificial neural network to predict the power and torque characteristics of a three-bucket Savonius rotor. Das et al. [54] use a hybrid differential evolution approach to estimate essential dimensions for a trapezoidal-shaped steel fin. Singla and Das [55] developed a differential evolution (DE)-based inverse analysis for optimizing the heat transfer rate from a rectangular stepped finned surface fulfilling a given volume. Das et al. [56] used the artificial bee colony (ABC) optimization method to perform an inverse study of a double-glazed flat-plate solar collector. Panda et al. [57] describe an analytical solution for a rectangular fin with simultaneous heat and mass transmission between the fin surface and the fin tip, and use inverse heat transfer analysis to determine the unknown thermal and geometrical configurations of the fin.

As obtaining an exact analytical solution to a problem might be complicated, the researcher uses a collection of numerical and semi-numerical techniques to tackle the problem. Keller Box Technique [58], HPM [59], Galerkin finite element method [60], Spectral Relaxation Method [61], as well as many others. All of the mentioned literature on nanofluid flow for several fluidic systems was invented using numerous numerical and semi numerical techniques; however, because of their advantage and efficiency, intelligence numerical computing models are essential to use the EMMN-PPRH model, i.e., the effects of electric and magnetic field on the micro-polar nano-fluid flow between two parallel plates with rotation under the influence of Hall current. Computational intelligence techniques have been utilized in stochastic numerical calculating solutions linked to artificial neural networks to obtain the results/outcomes of differential equations for linear and nonlinear, displaying varying capabilities under diverse conditions. The arrangement of such these techniques contains COVID-19 Models [56–63], electromagnetic [64], dust density model [65], atomic physics [66], entropy generation system [67], nonlinear Painlevé-I transcendent model [68], electrohydrodynamic pump flow system [69], nonlinear corneal shape model [60], Thomas–Fermi model [71], mosquito dispersal model [72], second grade nanofluidic system [73], and Emden–Fowler systems [74–76]. All of these motivating characteristics encourage researchers to use a dependable and accurate AI algorithm-based numerical computational model for numerical analysis of the Non-Newtonian Nano-fluid mathematical model by employing numerical and graphical evaluates to explore the effects of all alternatives or physical measures on the velocities, temperature, and concentration profiles. Package of Mathematica and MATLAB has been used to improve numerical accuracy.

The following are the key perspectives of the suggested design-computing methodology:

The (EMMN-PPRH) model, a new AI-based intelligent computing technique, was studied using an artificial neural network via the Levenberg–Marquardt backpropagation system (ANN-SLMB).
The mathematical modeling of the innovative scheme EMMN-PPRH in terms of PDEs has been translated to nonlinear ODEs by giving the appropriate analogous adjustment.
The HAM is used to construct a dataset for the suggested ANN-SLMB as an alternative to (EMMN-PPRH) to using the rotation parameter, the viscosity parameter, the coupling parameter, the Brownian motion parameter, the Prandtl number, and the electric parameter
The ANN-SLMB testing, validation, and training processes are used to model EMMN-PPRH for different scenarios, and evaluation with orientation outcomes rationalizes the accuracy of the recommended ANN-SLMB.
Convergence graphs of estimated MSE, fitness, histograms and regression metrics demonstrate the suitability of the suggested ANN-SLMB to appropriately describe the EMMN-PPRH model.

The following study is categorized as follows: in section two, the design and effects of the EMMN-PPRH model problem are presented. The solution approach, as well as the effects of the proposed ANN-SLMB on various scenarios of EMMN-PPRH, is presented in section three, and the final comments and potential future study are defined in the final unit.

## 2 Mathematical Modeling

Let us consider the movement of micro-polar, electrically conducting nano-fluid between both horizontal and parallel plates. The coordinate system is designed so that the plate and the fluid rotate around the $y$-axis at the same angular velocity $\Omega$. The distance between the top and lower plates is denoted by $h$. In order to extend the bottom plate down the $x$-axis, while maintaining the origin $O(0, 0, 0)$ constant, the two forces have to be of equal magnitude but opposite in direction. The upper plate has the ability to achieve constant wall suction velocity/injection $\overline{v}_0$. The fluid flow heat transfer is considered to be in a steady condition that is incompressible, laminar, and steady. In $y$-direction, a magnetic field $\overline{B}_0$ and an electric field $\overline{E}_0$ are operating. Furthermore, the micro-polar nano-fluid model considers the influence of Hall current. Figure 1 depicts the physical model. Whenever the magnetic field grows stronger, the fluids become electrically conducting, causing a Hall current to be generated, which influences the micro-polar nano-fluids. This

action increases the $z$-direction force, generating a flow distribution in the same direction and deflecting the micro-polar nano-fluid flows into 3 dimensions. The generalized Ohm's law, which includes the Hall current, is expressed as follows:

$$\overline{J} + \frac{\omega_e t_e}{B_0} \times \left(\overline{J} \times \overline{B}\right) - \frac{P_e \sigma_{nf}}{e n_e} - (\sigma_{nf})\left(\overline{V} \times \overline{B} + \overline{E}\right) = 0, \tag{1}$$

where $\overline{J} = (J_x, J_y, J_z)$ denotes current density and $\overline{J} = (\sigma_{nf})(\overline{V} \times \overline{B} + \overline{E})$, $\overline{E}$ denotes the electric field intensity $(0, E_0, 0) = \overline{E}$, $\overline{V}(\overline{u}, \overline{v}, \overline{w})$ denotes components of velocity, $\overline{B} = (0, B_0, 0)$ indicates magnetic field, $\omega_e$ indicates oscillating frequency of the electron, $t_e$ denotes the times of electron collision, $P_e$ is the pressure of the electron, $\sigma_{nf}$ represent electrical conductivity, $n_e$ is the number density of electron and $e$ is stand for charge of electron. Considering the inherent parameters, the Ohm law in generalized form offers $\left(J_y = 0\right)$ in the flow field for weakly ionized molecules. Using these assumptions, we get $J_x$ and $J_z$ as [10–17]:

$$J_x = \frac{\sigma_{nf} \overline{B}_0^2}{1 + m^2}(m\overline{u} - \overline{w}), \tag{2}$$

$$J_z = \frac{\sigma_{nf} \overline{B}_0^2}{1 + m^2}(\overline{u} + m\overline{w}). \tag{3}$$

Here, $m = t_e \omega_e$ represents the Hall parameter.

By suppositions stated above, the continuity and momentum equations are reduced to [19–28]:

$$\frac{\partial \overline{v}}{\partial y} + \frac{\partial \overline{u}}{\partial x} = 0, \tag{4}$$

$$\frac{\partial \overline{u}}{\partial y}.\overline{v} + \frac{\partial \overline{u}}{\partial x} \cdot \overline{u} = -\frac{1}{\rho_f}\frac{\partial \widehat{p}}{\partial x} + \left(\frac{\widehat{\kappa}}{\rho_f} + \nu\right)\left(\frac{\partial^2 \overline{u}}{\partial x^2} + \frac{\partial^2 \overline{u}}{\partial y^2}\right) - 2\overline{w}\,\Omega + \frac{\widehat{\kappa}}{\rho_f}\frac{\partial \overline{N}}{\partial y} - \frac{\overline{B}_0^2 \sigma_{nf}}{m^2 + 1}\frac{1}{\rho_f}(m\overline{w} + \overline{u}) - \frac{\sigma_{nf}\overline{B}_0 \overline{E}_0}{\rho_f}, \tag{5}$$

$$\frac{\partial \overline{v}}{\partial x} \cdot \overline{u} + \frac{\partial \overline{v}}{\partial y} \cdot \overline{v} = -\frac{1}{\rho_f}\frac{\partial \widehat{p}}{\partial x} + \left(\frac{\partial^2 \overline{v}}{\partial y^2} + \frac{\partial^2 \overline{v}}{\partial x^2}\right) + \frac{\widehat{\kappa}}{\rho_f}\frac{\partial \overline{N}}{\partial x}, \tag{6}$$

$$\frac{\partial \overline{w}}{\partial x} \cdot (\overline{u}) + \frac{\partial \overline{w}}{\partial y} \cdot (\overline{v}) = \left(\frac{\widehat{\kappa}}{\rho_f} + \nu\right)\left(\frac{\partial^2 \overline{w}}{\partial x^2} + \frac{\partial^2 \overline{w}}{\partial y^2}\right) + 2\overline{u}\Omega + \frac{\sigma_{nf}\overline{B}_0^2}{1 + m^2}\frac{1}{\rho_f}(m\overline{u} - \overline{w}) + \frac{\sigma_{nf}\overline{B}_0 \overline{E}_0}{\rho_f}. \tag{7}$$

From Eqs. (4)–(7), $v$, $\mu$denotes the kinematic and dynamic viscosities coefficient, respectively, $\Omega$ represents angular velocity, $\widehat{\kappa}$ denotes vertex viscosity, $\rho_f$ indicates the base fluid density, and $\overline{N}$ is stand for the micro-rotation angular velocity.

The equation of energy is become as [36–39]:

$$\frac{\partial T}{\partial x} \cdot (u) + \frac{\partial T}{\partial y} \cdot (v) + \frac{\partial T}{\partial z} \cdot (w) = \alpha^*\left(\frac{\partial^2 T}{\partial x^2} + \frac{\partial^2 T}{\partial y^2} + \frac{\partial^2 T}{\partial z^2}\right)\tau^*\left[D_B\left\{\frac{\partial C}{\partial x}\frac{\partial T}{\partial x} + \frac{\partial C}{\partial y}\frac{\partial T}{\partial y} + \frac{\partial C}{\partial z}\frac{\partial T}{\partial z}\right\} + \frac{D_T}{T_C}\left\{\left(\frac{\partial T}{\partial x}\right)^2 + \left(\frac{\partial T}{\partial z}\right)^2 + \left(\frac{\partial T}{\partial y}\right)^2\right\}\right]. \tag{8}$$

The equation of micro-rotation angular velocity is become as [19–28]:

$$\frac{\partial \overline{N}}{\partial x} \cdot (\overline{u}) + \frac{\partial \overline{N}}{\partial y} \cdot (\overline{v}) = -\gamma \cdot \frac{1}{\rho_j}\left(\frac{\partial^2 \overline{N}}{\partial x^2} + \frac{\partial^2 \overline{N}}{\partial y^2}\right) + \frac{\widehat{\kappa}}{\rho_j}\left(\frac{\partial \overline{v}}{\partial x} - \frac{\partial \overline{u}}{\partial y}\right) - \frac{2\widehat{\kappa}\overline{N}}{\rho_j}. \tag{9}$$

Mass transfer equation is become as [36–39]:

$$\frac{\partial C}{\partial x} \cdot (u) + \frac{\partial C}{\partial y} \cdot (v) + \frac{\partial C}{\partial z} \cdot (w) = (D_B) \cdot \left(\frac{\partial^2 C}{\partial z^2} + \frac{\partial^2 C}{\partial y^2} + \frac{\partial^2 C}{\partial x^2}\right) + D_T \cdot \frac{1}{T_0} \cdot \left(\frac{\partial^2 T}{\partial z^2} + \frac{\partial^2 T}{\partial y^2} + \frac{\partial^2 T}{\partial x^2}\right). \tag{10}$$

Here in Eq. (8), $\alpha^*$ denotes thermal diffusivity, $T$ denotes temperature, $\tau^* = (\rho c)_p / (\rho c)_f$ is defined as the ratios of nanoparticles and effective heat capacity, $D_B$ denotes the Brownian diffusion coefficients, $D_T$ denotes thermophoretic diffusion coefficient, $c_p$ denotes specific heat, and $C$ is stand for the fluid concentration of the fluids particles. The boundary conditions for the state problem are as follows:

$$\overline{v} = 0,\ \overline{u} = \alpha x,\ \overline{w} = 0,\ T = T_h,\ C = C_h,\ \overline{N} = -k\frac{\partial \overline{u}}{\partial y},\ \text{at } y = 0,$$
$$\overline{u} = \overline{v} = \overline{w} = 0,\ T = T_0,\ C = C_0,\ \overline{N} = k\frac{\partial \overline{u}}{\partial y}\ \text{when } y = h. \tag{11}$$

The boundary parameter is denoted by $k$. The fluid flow is the turbulent, weak, and strong concentration when the valve of $k = 1.0$, $k = 1/2$ and $k = 0$, respectively. The dimensionless variables are represented as follows:

$$\overline{N} = -\frac{\alpha x G(\eta)}{h},\ \overline{u} = \alpha x f'(\eta),\ \overline{w} = \alpha x g(\eta),\ \overline{v} = -\alpha h f(\eta),$$
$$\Theta(\eta) = \frac{T - T_h}{T_0 - T_h},\ \Phi(\eta) = \frac{C - C_h}{C_0 - C_h},\ \text{where } \eta = \frac{y}{h}. \tag{12}$$

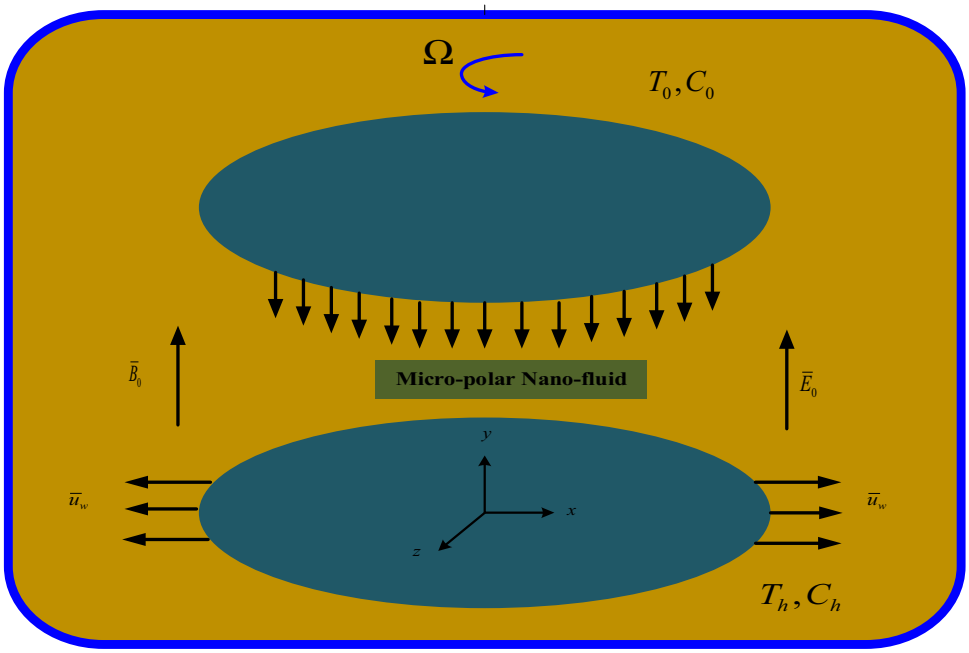


**Fig. 1** Micro-polar nano-fluid geometry

when the dimensionless variables from Eq. (12) are replaced by Eqs. (4)–(10), (4) remains identical, and the other governing Eqs. (5)–(10) are simplified to the form of

$$(1+N_1)f^{iv} - \mathrm{Re}\left(f'f'' - ff'''\right) + \frac{M}{1+m^2}\left(f'' + mg'\right) - 2Krg' + N_1G'' + MEI = 0, \tag{13}$$

$$(1+N_1)g'' - \mathrm{Re}\left(fg' - gf'\right) + 2Krf' + \frac{M}{1+m^2}\left(mf' - g\right) - MEI = 0, \tag{14}$$

$$\Theta'' + \mathrm{Pr}\left(\mathrm{Re}\, f\Theta' + Nb\Phi'\Theta' + Nt\Theta'^2\right) = 0, \tag{15}$$

$$N_2G'' - N_1\left(2G + f''\right) - N_3\mathrm{Re}\left(Gf' - G'f\right) = 0, \tag{16}$$

$$\Phi'' + \mathrm{Re}Scf\Phi' + \frac{Nt}{Nb}\Theta'' = 0. \tag{17}$$

When the dimensionless variable from Eq. (12) is utilized in it, Eq. (11) is simplified to the following form:

$$\begin{aligned} &f = 0,\ f' = 1,\ g = 0,\ \Theta = 1,\ G = -kf'',\ \Phi = 1,\ \text{at}\,\eta = 0 \\ &f = \delta,\ f' = 0,\ g = 0,\ \Theta = 0,\ G = kf'',\ \Phi(1) = 0,\ \text{when}\,\eta = 1. \end{aligned} \tag{18}$$

The dimensional physical parameters after simplification are as follows:

$$\mathrm{Re} = \frac{ah^2}{v},\ \mathrm{EI} = \frac{E_0}{B_0ax},\ \mathrm{Kr} = \frac{2\Omega h^2}{v},$$

$$M = \frac{\sigma_{nf}h^2B_0^2}{\rho v},\ N_1 = \frac{\widehat{\kappa}}{\mu},\ N_2 = \frac{v_s}{vh^2},\ N_3 = \frac{j}{h^2},$$
$$\mathrm{Pr} = \frac{\mu}{\rho_f\alpha},\ \mathrm{Nb} = \frac{(\rho c)_pD_BC_h}{\alpha^*(\rho c)_f},\ \mathrm{Nt} = \frac{(\rho c)_pD_TT_0}{(\rho c)_fT_c},$$
$$\mathrm{Sc} = \frac{\mu}{D\rho_f},\ \delta = \frac{v_0}{h}. \tag{19}$$

where $N_1$ denotes the coupling parameter, Kr denotes rotation parameter, $M$ is stand for magnetic parameter, $N_2$ represents spin gradient viscosity parameter, EI is stand for electric parameter, $\delta$ denotes transpiration parameter, $N_3$ is stand for micro-polar fluid constant, Re is stand for viscosity parameter, PR indicates Prandtl number, Nt denotes thermophoretic parameter, Sc indicates the Schmidt number, and Nb indicates the Brownian motion parameter.

Here, $C_f = \frac{(\overline{S}_{xy})_{y=0}}{\rho\bar{u}_w^2}$ represents the skin friction, where $\overline{S}_{xy} = \left((\mu+\widehat{\kappa})\frac{\partial u}{\partial y} + \widehat{\kappa}N\right)$, $Q_w$ is the heat flux and $Q_w = \left(\frac{\partial T}{\partial y}\right)_{y=0}(-\overline{k})$, the Nusselt number is expressed as $Nu = \frac{hQ_w}{\widehat{k}(T_0-T_h)}$. The number of Sherwood is expressed as $Sh = \frac{hJ_w}{D_B(C_0-C_h)}$, $J_w$ is the mass flux and $J_w = (-D_B)\left(\frac{\partial C}{\partial y}\right)_{y=0}$. $C_f$, $Nu$ and $Sh$ are achieved in the dimensionless form as

$$C_f\sqrt{\mathrm{Re}_x} = N_1G(0) + (1+N_1)f''(0),$$
$$\mathrm{Nu} = -\Theta'(0),\ \mathrm{Sh} = -\Phi'(0). \tag{20}$$

wherever $\mathrm{Re}_x$ stands for local Reynolds number and is denoted by $\mathrm{Re}_x = \frac{\bar{u}_wx}{v}$.

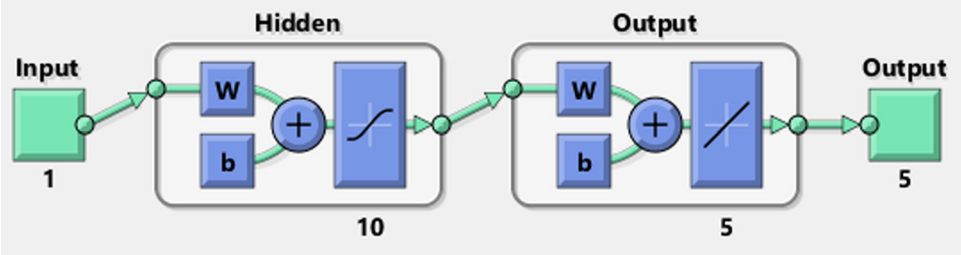


**Fig. 2** Neural Network Design for EMMN-PPRH model

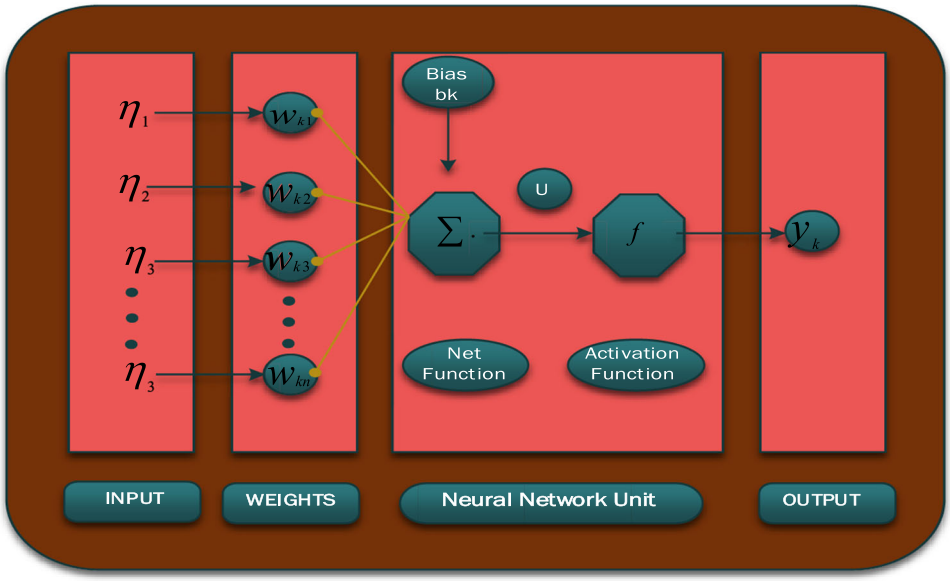


**(a)** Configuration of a specific neural framework

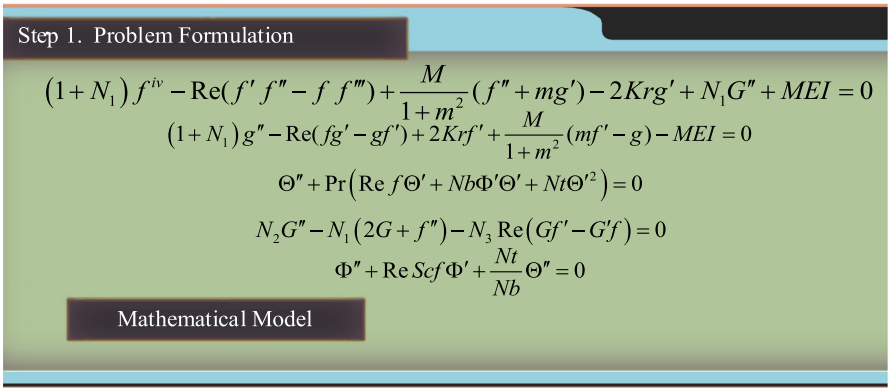


**(b)** EMMN-PPRH Mathematical Model

**Fig. 3** (**a**) Configuration of a specific neural framework. (**b**) EMMN-PPRH Mathematical Model

## 3 Solution Approach and Assessment

The recommended ANN-SLMB in the configuration of a neural network is depicted in Fig. 2. The recommended ANN-SLMB is conducted using the 'nf tool,' which is a technique for fitting NN tools in MATLAB's neural network (NN) toolbox, while backpropagation of Levenberg–Marquardt is used to determine the weight of neural networks. The proposed ANN-SLMB framework is shown in Fig. 3a, and the mathematical model is shown in Fig. 3b, while the overall extension of the flow is shown in Fig. 4.

Figures 5, 6, 7, 8, 9, 10, 11, 12, 13 show the ANN-SLMB implications for the EMMN-PPRH model in different scenarios (1 to 6). Figures 5 and 6 show the outcomes of six scenarios $M$, $kr$, $R$, $Rd$, $Sc$ and $Nt$ in form of execution and transition phases. The fitting plots and error histograms in Figs. 7, 8 are discussed in expressions of solution with error for four distinct cases, whereas regression assessments

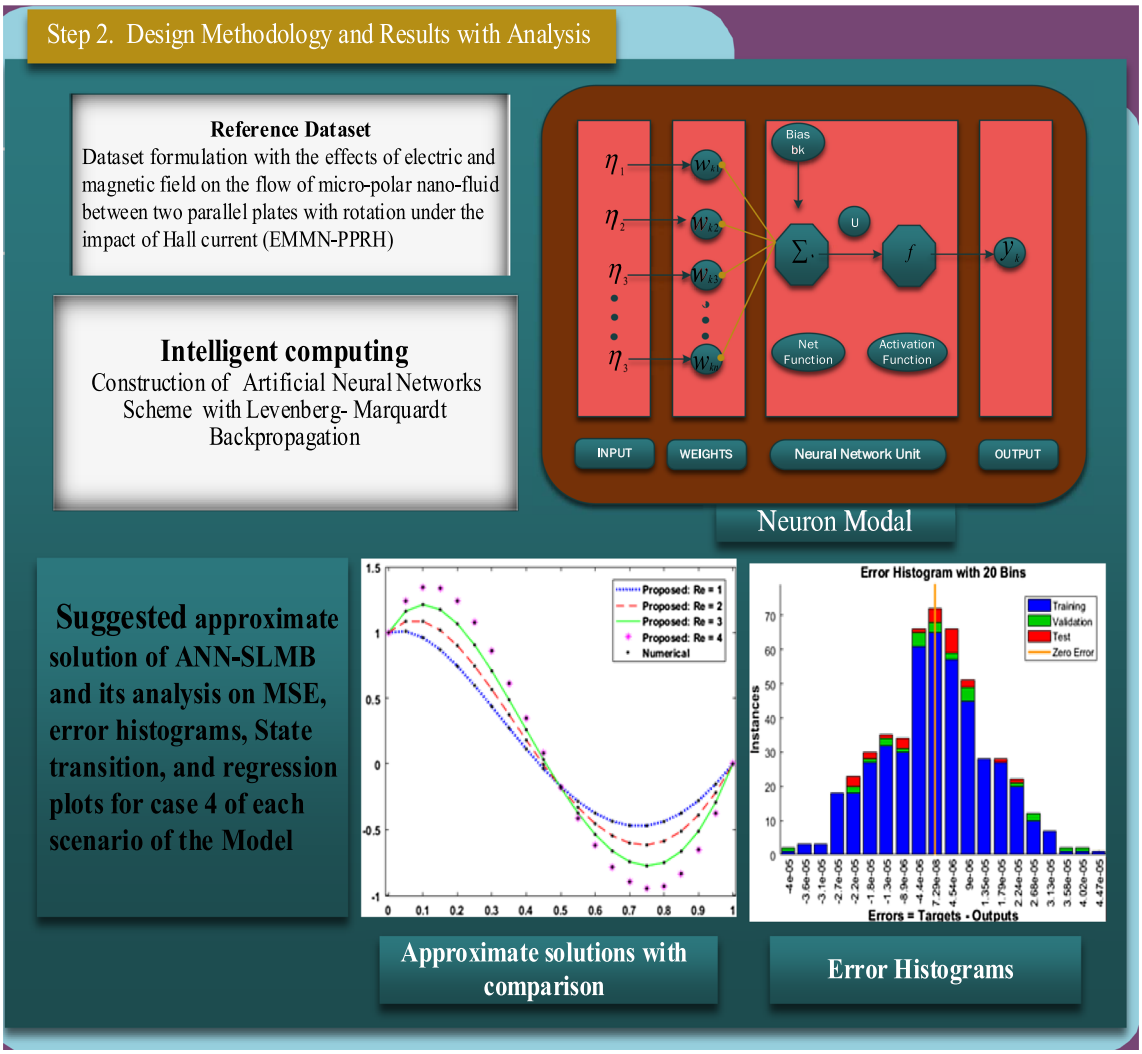


**Fig. 4** The suggested ANN-SLMB workflow procedure for the EMMN-PPRH model

in Figs. 9, 10, 11 are exhibited for four distinct cases of the EMMN-PPRH model. Furthermore, for each EMMN-PPRH model scenario, the convergence achieves parameter in form of MSE, execution, performance duration, executed period, and gauges of backpropagation and behavioral convolution are included in Tables (2–7) for all 6 scenarios, respectively.

Figures 5, 6a, c, e for test procedures indicated the MSE convergence, training, and validation improvements for six scenarios of the EMMN-PPRH model. The best network performance was achieved with MSE close to $2.19 \times 10^{-10}$, $2.12 \times 10^{-10}$, $2.47 \times 10^{-10}$, $2.37 \times 10^{-10}$, $2.56 \times 10^{-10}$ and $1.82 \times 10^{-10}$. The reduced the MSE figure, the more precise and accurate the execution of the recommended approach. The concerning values of step size Mu and gradient of Levenberg–Marquardt are finely [$1.00 \times 10^{-08}$, $1.00 \times 10^{-08}$, $1.00 \times 10^{-08}$, $1.00 \times 10^{-08}$, $1.00 \times 10^{-08}$ and $1.00 \times 10^{-08}$] and [$9.97 \times 10^{-08}$, $9.97 \times 10^{-08}$, $9.97 \times 10^{-08}$, $9.96 \times 10^{-08}$, $9.95 \times 10^{-08}$ and $9.97 \times 10^{-08}$] are existent in Figs. 5, 6b, d, f. The results and graphical illustrations above demonstrate that ANN-SLMB is competent, accurate, and convergent for case 4 of the EMMN-PPRH model.

Figures 7, 8 assess the efficiency of the EMMN-PPRH model by analyzing the created consequences of six distinct scenarios for inputs ranging from 0 to 1 with a step range of 0.01 with reference numerical results of HAM and related outcomes, as well as the design of error dynamics. The greatest error for the test, train, and validation statistics achieved via recommended ANN-SLMB is less than $3.70 \times 10^{-10}$, $3.34 \times 10^{-10}$, $7.18 \times 10^{-10}$, $2.90 \times 10^{-10}$, $4.16 \times 10^{-10}$ and $2.85 \times 10^{-10}$, whereas the error dynamics and results of the EMMN-PPRH model for 6 different scenarios are also analyzed for each input point apart from the error histograms are demonstrated in Figs. 7, 8a, b, c, respectively. The average value of error bin via compared zero line has errors about $7.29 \times 10^{-08}$, $7.29 \times 10^{-08}$, $-1.9 \times 10^{-06}$, $5 \times 10^{-08}$, 2.04

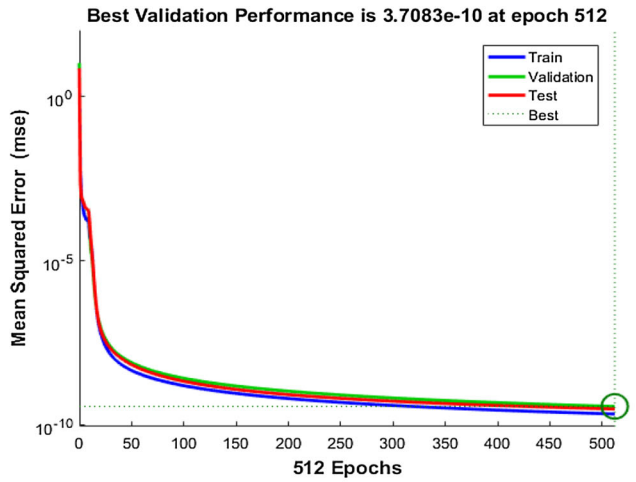


(a) Effects of MSE for C4 of S1

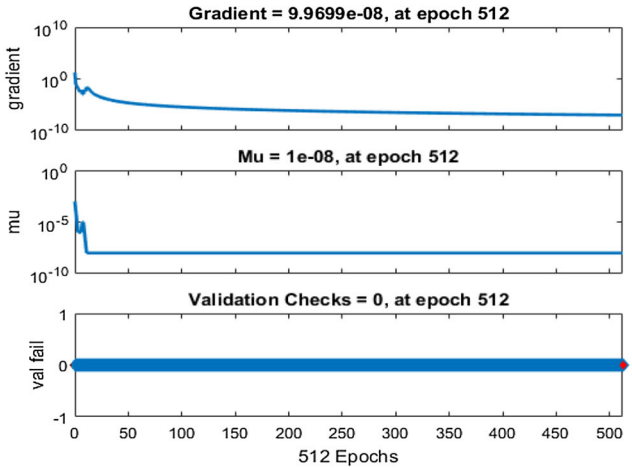


(b) Effects of State transition for C4 of S1

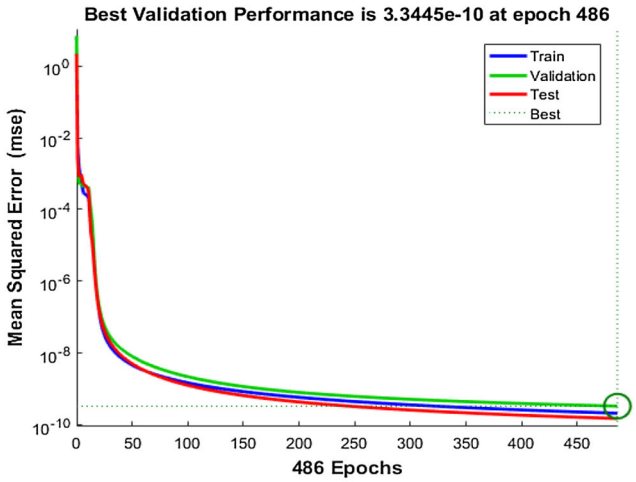


(c) Effects of MSE for C4 of S2

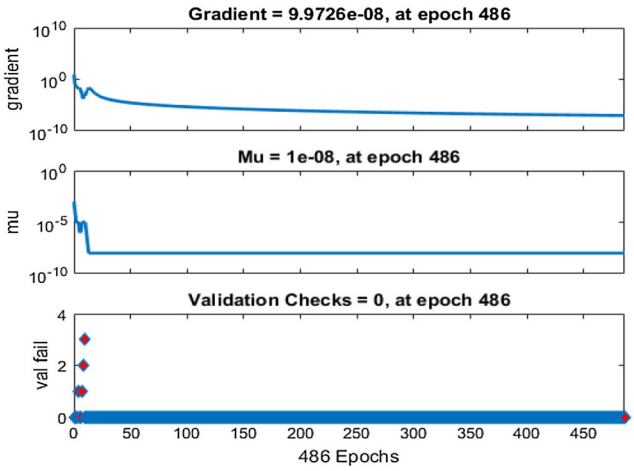


(d) Effects of State transition for C4 of S2

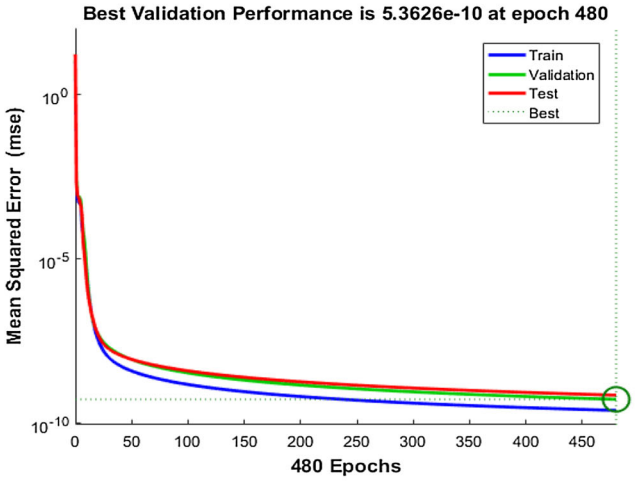


(e) Effects of MSE for C4 of S3

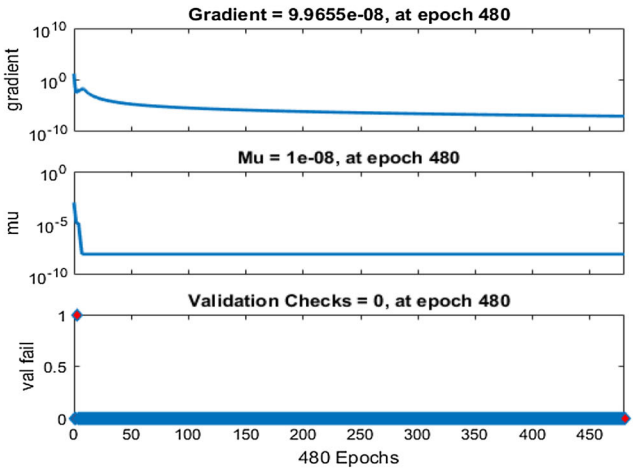


(f) Effects of State transition for C4 of S3

**Fig. 5** Performance solution and State transition of Recommended ANN-SBLM for solving EMMN-PPRH model for case 4 of scenarios 1, 2 and 3

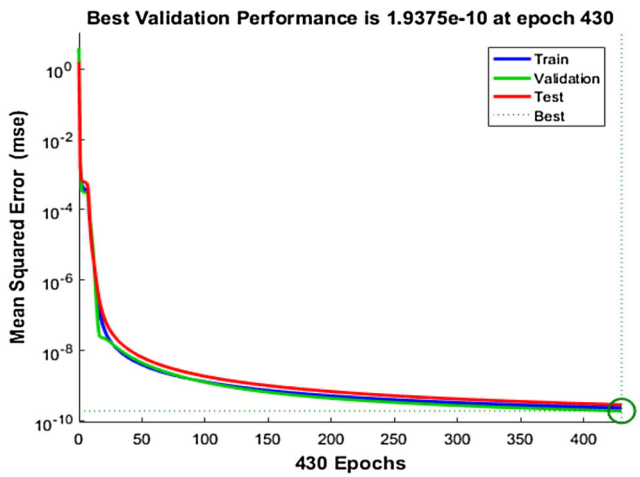


(a) Effects of MSE for C4 of S4

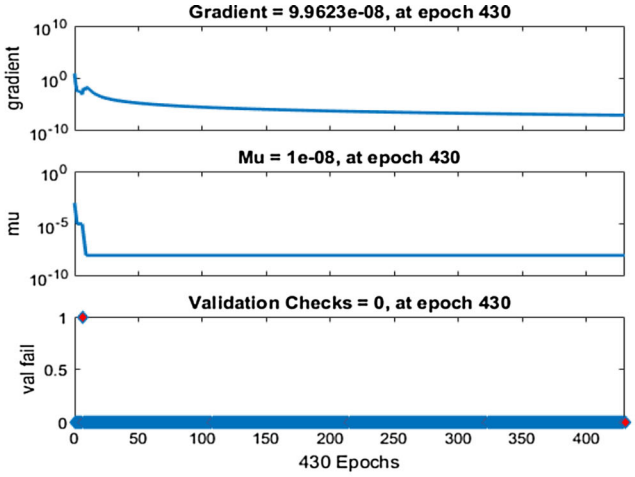


(b) Effects of State transition for C4 of S4

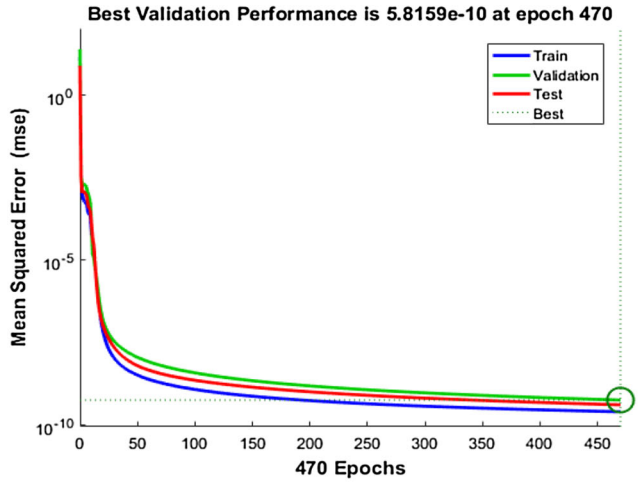


(c) Effects of MSE for C4 of S5

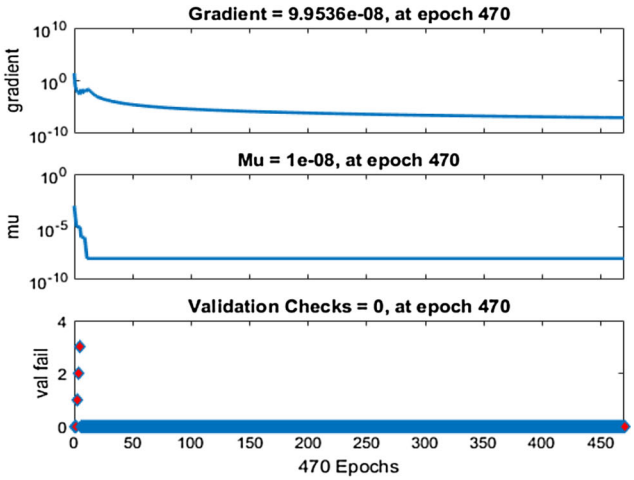


(d) Effects of State transition for C4 of S5

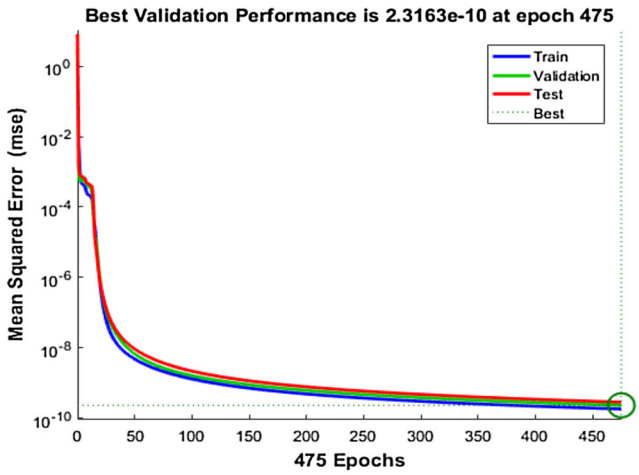


(e) Effects of MSE for C4 of S6

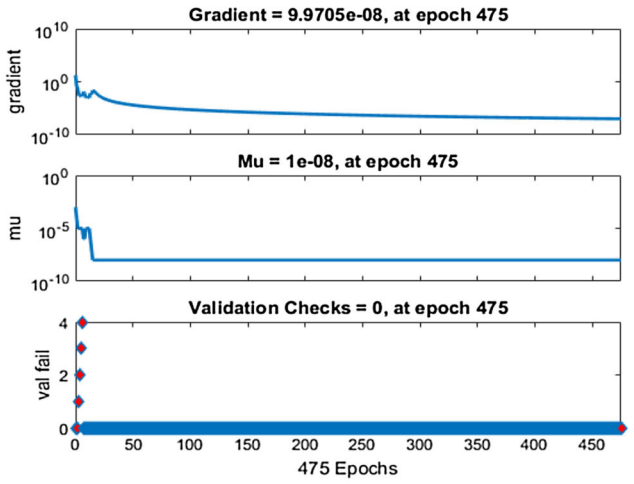


(f) Effects of State transition for C4 of S6

**Fig. 6** Performance solution and State transition of Recommended ANN-SBLM for solving EMMN-PPRH model for case 4 of scenarios 4, 5 and 6

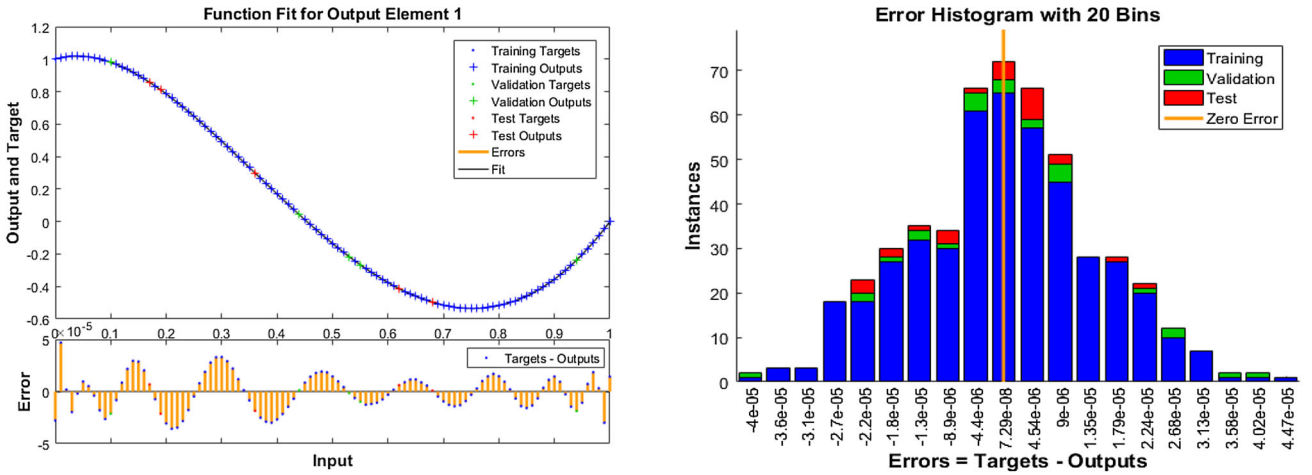


**(a)** Effects of Fitness and E.H for C4 of S1

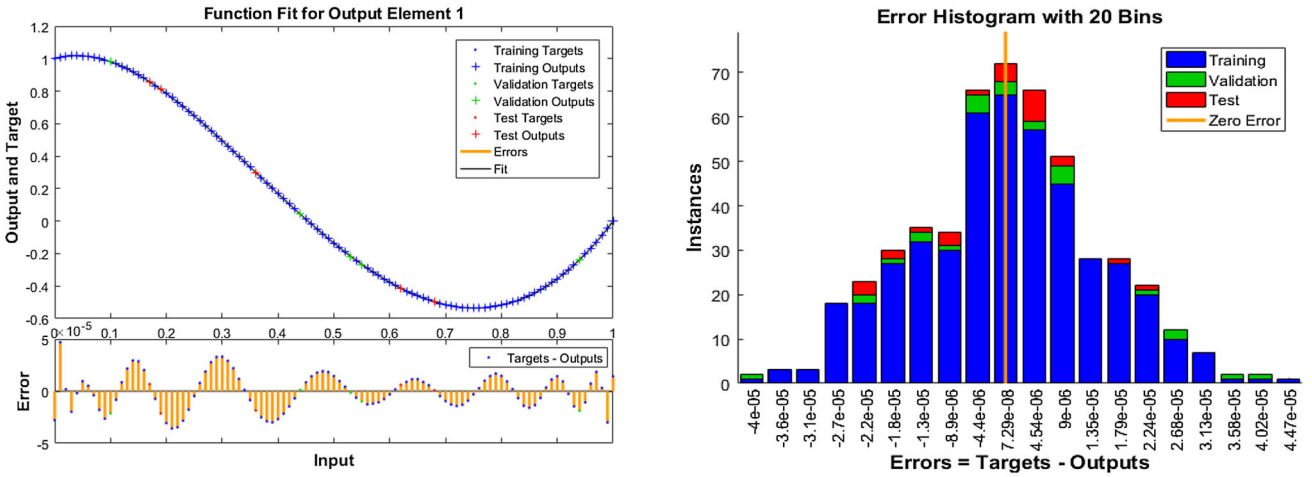


**(b)** Effects of Fitness and E.H for C4 of S2

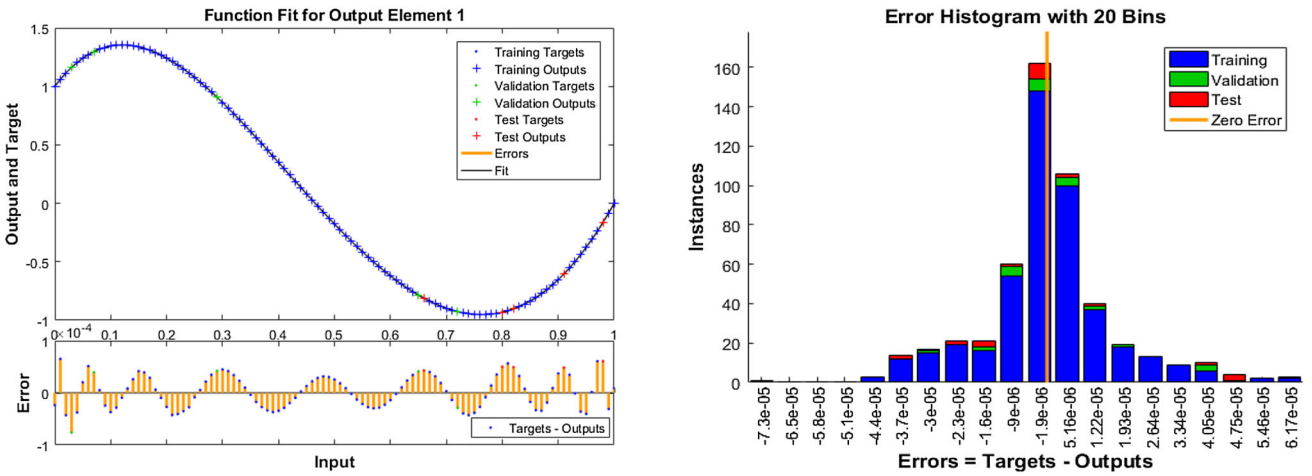


**(c)** Effects of Fitness and E.H for C4 of S3

**Fig. 7** Solution of Fitness and Error analysis of Recommended ANN-SBLM for solving EMMN-PPRH model for case 4 of scenarios 1, 2 and 3

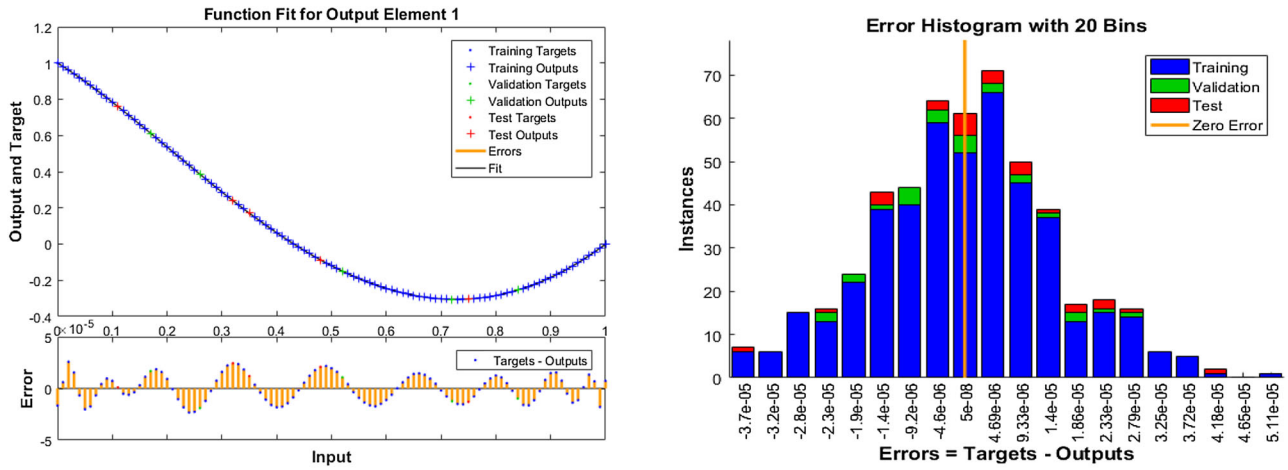


**(a)** Effects of Fitness and E.H for C4 of S4

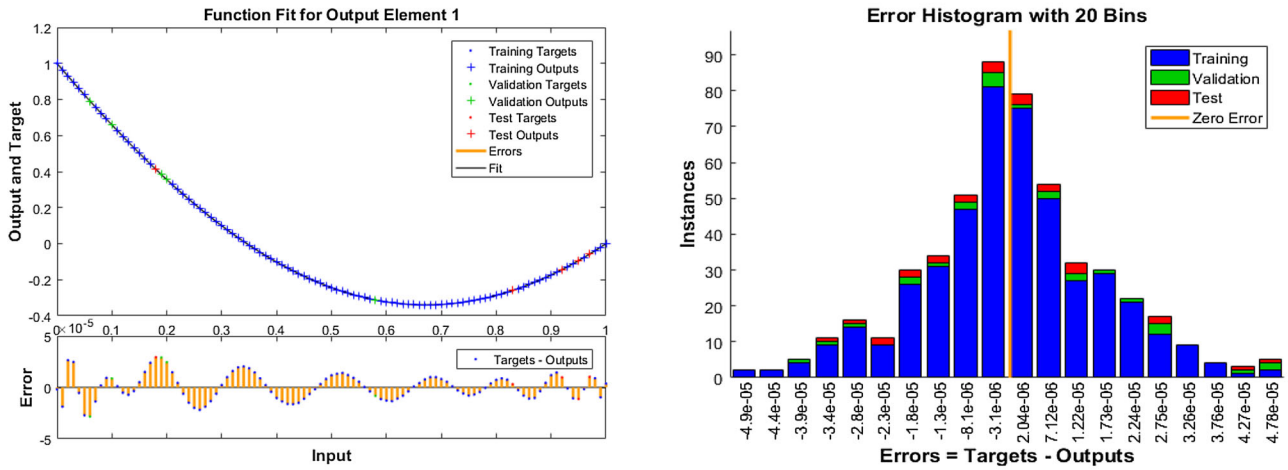


**(b)** Effects of Fitness and E.H for C4 of S5

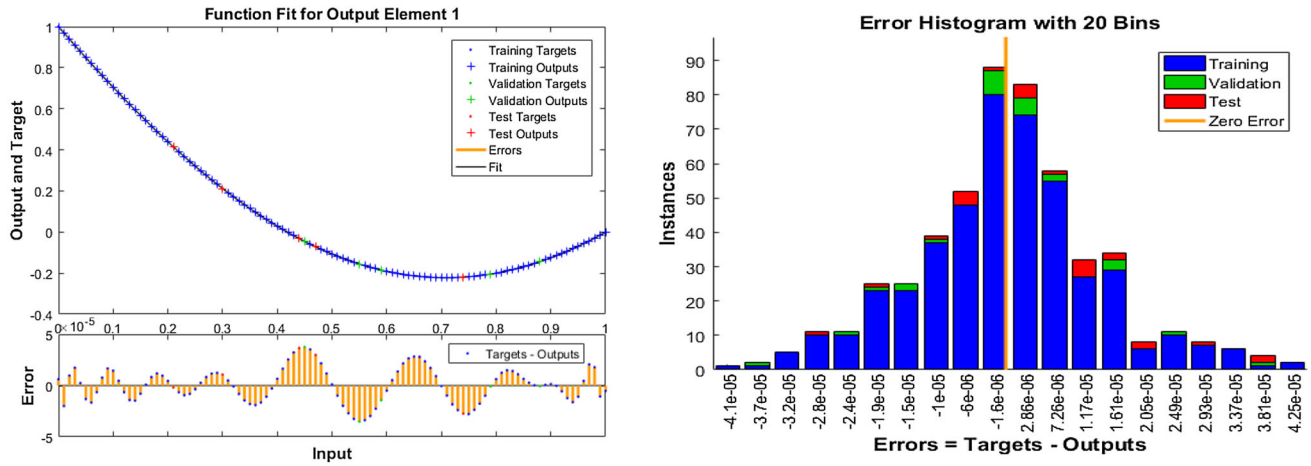


**(c)** Effects of Fitness and E.H for C4 of S6

**Fig. 8** Solution of Fitness and Error analysis of Recommended ANN-SBLM for solving EMMN-PPRH model for case 4 of scenarios 4, 5 and 6

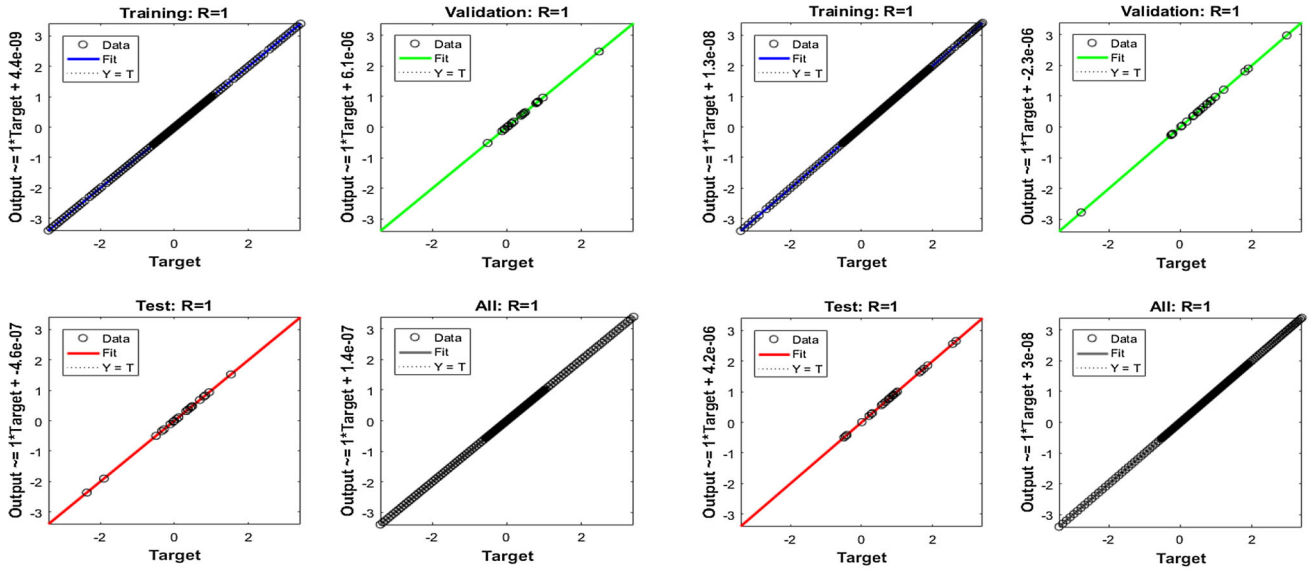


**(a)** Effects of Regression for C4 of S1 **(b)** Effects of Regression for C4 of S2

**Fig. 9** Regression effectiveness of the Recommended ANN-SBLM for solving EMMN-PPRH model for case 4 of scenarios 1 and 2

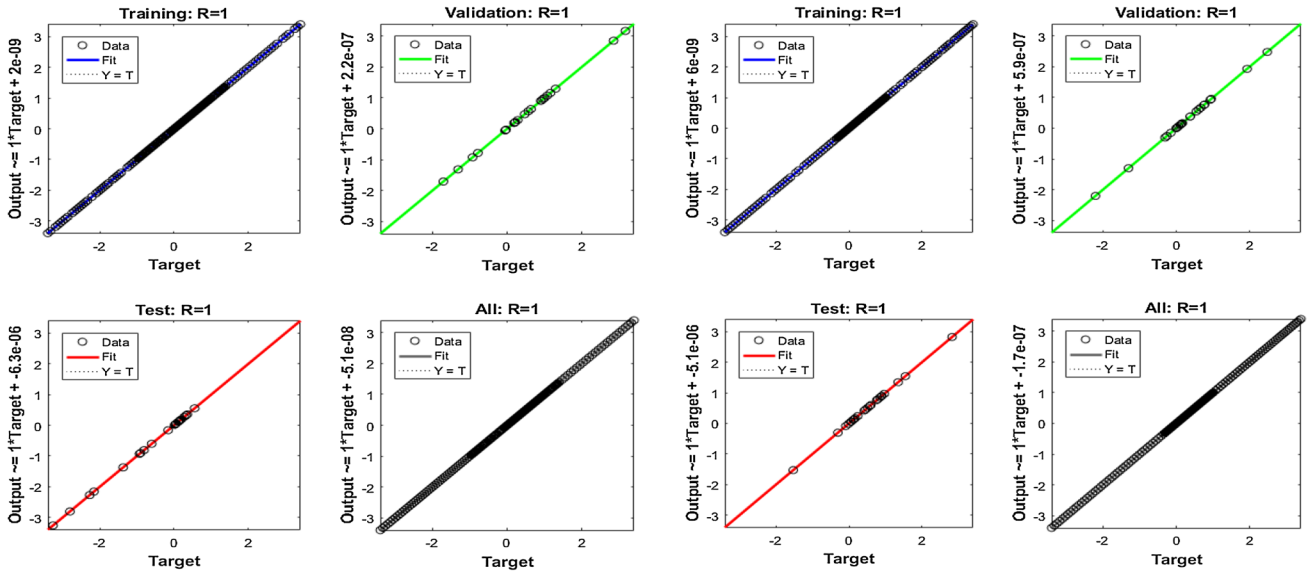


**(a)** Effects of Regression for C4 of S3 **(b)** Effects of Regression for C4 of S4

**Fig. 10** Regression effectiveness of the Recommended ANN-SBLM for solving EMMN-PPRH model for case 4 of scenarios 3 and 4

$\times\ 10^{-06}$ and $-\ 1.6 \times 10^{-06}$ for case 4 of all 6 distinct scenarios of the model, EMMN-PPRH. Co-relation analyses are commonly used to classify the investigation inside regression analyses. Figures 9, 10, 11 show the effects of the EMMN-PPRH model's related six scenarios. Correlation values are constantly near to unity, indicating that this is the optimal value for validation, training, and testing for precise modeling, which indicates how effectively ANN-SLMB resolves the EMMN-PPRH model.

Furthermore, for various EMMN-PPRH model parameters (1–6), the associated numerical data in Table 2, 3, 4, 5, 6, 7 demonstrate that MSE efficiency for the proposed ANN-SLMB technique is close 1E−10. The numerical results in Tables 2, 3, 4, 5, 6, 7 demonstrate that ANN-SLMB solves the EMMN-PPRH model well.

The results of ANN-SLMB are validated for velocities $f'(\eta)$ and $g(\eta)$, and temperature $\Theta(\eta)$ profiles for scenarios 1–6 of the EMMN-PPRH paradigm are presented in Figs. 12 and 13, respectively. The influence of velocity profiles $f'(\eta)$

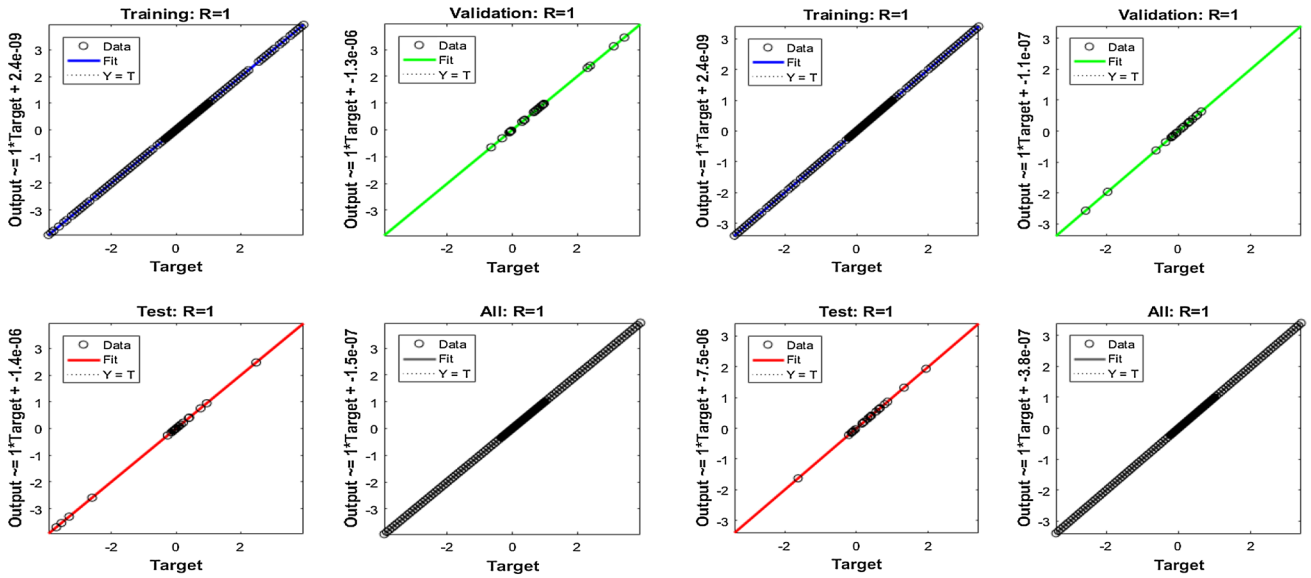


**(a)** Effects of Regression for C4 of S5 **(b)** Effects of Regression for C4 of S6

**Fig. 11** Regression effectiveness of the Recommended ANN-SBLM for solving EMMN-PPRH model for case 4 of scenarios 5 and 6

**Table 1** Depiction of all scenarios along with 4 different cases for the EMMN-PPRH model

| Scenarios | Case | Interest physical quantities | | | | | | | | | | | | | |
|---|---|---|---|---|---|---|---|---|---|---|---|---|---|---|---|
| | | Kr | EI | Re | $N_1$ | Nb | Pr | $M$ | $m$ | Nt | $N_2$ | $N_3$ | Sc | $\delta$ | $k$ |
| S1 | C1 | 0.5 | 0.6 | 1 | 1.5 | 0.8 | 1.5 | 1 | 0.6 | 0.3 | 1.5 | 1 | 0.8 | 0.1 | 1 |
| | C2 | 1.0 | 0.6 | 1 | 1.5 | 0.8 | 1.5 | 1 | 0.6 | 0.3 | 1.5 | 1 | 0.8 | 0.1 | 1 |
| | C3 | 1.5 | 0.6 | 1 | 1.5 | 0.8 | 1.5 | 1 | 0.6 | 0.3 | 1.5 | 1 | 0.8 | 0.1 | 1 |
| | C4 | 2.0 | 0.6 | 1 | 1.5 | 0.8 | 1.5 | 1 | 0.6 | 0.3 | 1.5 | 1 | 0.8 | 0.1 | 1 |
| S2 | C1 | 0.8 | 1 | 1 | 2 | 0.8 | 1.5 | 1 | 0.6 | 0.3 | 2 | 1 | 0.8 | 0.1 | 1 |
| | C2 | 0.8 | 2 | 1 | 2 | 0.8 | 1.5 | 1 | 0.6 | 0.3 | 2 | 1 | 0.8 | 0.1 | 1 |
| | C3 | 0.8 | 3 | 1 | 2 | 0.8 | 1.5 | 1 | 0.6 | 0.3 | 2 | 1 | 0.8 | 0.1 | 1 |
| | C4 | 0.8 | 4 | 1 | 2 | 0.8 | 1.5 | 1 | 0.6 | 0.3 | 2 | 1 | 0.8 | 0.1 | 1 |
| S3 | C1 | 0.8 | 0.6 | 1 | 2 | 0.8 | 1.5 | 1 | 0.6 | 0.3 | 2 | 2 | 0.8 | 0.1 | 1 |
| | C2 | 0.8 | 0.6 | 2 | 2 | 0.8 | 1.5 | 1 | 0.6 | 0.3 | 2 | 2 | 0.8 | 0.1 | 1 |
| | C3 | 0.8 | 0.6 | 3 | 2 | 0.8 | 1.5 | 1 | 0.6 | 0.3 | 2 | 2 | 0.8 | 0.1 | 1 |
| | C4 | 0.8 | 0.6 | 4 | 2 | 0.8 | 1.5 | 1 | 0.6 | 0.3 | 2 | 2 | 0.8 | 0.1 | 1 |
| S4 | C1 | 0.8 | 0.6 | 1 | 0.1 | 0.8 | 1.5 | 1 | 0.6 | 0.3 | 1 | 1 | 0.8 | 0.1 | 1 |
| | C2 | 0.8 | 0.6 | 1 | 1.0 | 0.8 | 1.5 | 1 | 0.6 | 0.3 | 1 | 1 | 0.8 | 0.1 | 1 |
| | C3 | 0.8 | 0.6 | 1 | 1.5 | 0.8 | 1.5 | 1 | 0.6 | 0.3 | 1 | 1 | 0.8 | 0.1 | 1 |
| | C4 | 0.8 | 0.6 | 1 | 2.0 | 0.8 | 1.5 | 1 | 0.6 | 0.3 | 1 | 1 | 0.8 | 0.1 | 1 |
| S5 | C1 | 0.8 | 0.6 | 1 | 1 | 0.1 | 1.5 | 1 | 0.6 | 0.3 | 2 | 1 | 0.8 | 0.1 | 1 |
| | C2 | 0.8 | 0.6 | 1 | 1 | 0.3 | 1.5 | 1 | 0.6 | 0.3 | 2 | 1 | 0.8 | 0.1 | 1 |
| | C3 | 0.8 | 0.6 | 1 | 1 | 0.5 | 1.5 | 1 | 0.6 | 0.3 | 2 | 1 | 0.8 | 0.1 | 1 |
| | C4 | 0.8 | 0.6 | 1 | 1 | 0.7 | 1.5 | 1 | 0.6 | 0.3 | 2 | 1 | 0.8 | 0.1 | 1 |
| S6 | C1 | 0.8 | 0.6 | 1 | 1 | 0.5 | 1 | 1 | 0.6 | 0.3 | 2 | 1 | 0.8 | 0.1 | 1 |
| | C2 | 0.8 | 0.6 | 1 | 1 | 0.5 | 2 | 1 | 0.6 | 0.3 | 2 | 1 | 0.8 | 0.1 | 1 |
| | C3 | 0.8 | 0.6 | 1 | 1 | 0.5 | 3 | 1 | 0.6 | 0.3 | 2 | 1 | 0.8 | 0.1 | 1 |
| | C4 | 0.8 | 0.6 | 1 | 1 | 0.5 | 4 | 1 | 0.6 | 0.3 | 2 | 1 | 0.8 | 0.1 | 1 |

**Table 2** ANN-SLMB consequence of the EMMN-PPRH model for Scenario 1

| Case | MSE | | | Execution | Gradient | Mu | Epoch | Time |
|---|---|---|---|---|---|---|---|---|
| | MSE training | MSE validation | MSE testing | | | | | |
| C1 | 1.6506E−11 | 2.5701E−11 | 2.0446E−10 | 1.65E−11 | 9.97E−08 | 1.00E−09 | 441 | 1 |
| C2 | 2.2740E−10 | 2.4744E−10 | 3.4024E−10 | 2.27E−10 | 9.99E−08 | 1.00E−08 | 504 | 1 |
| C3 | 1.9755E−11 | 2.1231E−11 | 2.6966E−11 | 1.98E−11 | 9.97E−08 | 1.00E−09 | 409 | 1 |
| C4 | 2.1852E−10 | 3.7083E−10 | 3.0959E−10 | 2.19E−10 | 9.97E−08 | 1.00E−08 | 512 | 1 |

**Table 3** ANN-SLMB consequence of the EMMN-PPRH model for Scenario 2

| Case | MSE | | | Execution | Gradient | Mu | Epoch | Time |
|---|---|---|---|---|---|---|---|---|
| | MSE training | MSE validation | MSE testing | | | | | |
| C1 | 2.0306E−10 | 2.9670E−10 | 3.7321E−10 | 1.73E−10 | 9.97E−08 | 1.00E−08 | 492 | 1 |
| C2 | 1.7326E−10 | 2.6433E−10 | 2.8741E−10 | 1.30E−10 | 9.97E−08 | 1.00E−08 | 472 | 1 |
| C3 | 1.9992E−10 | 3.6165E−10 | 5.4846E−10 | 2.00E−10 | 9.99E−08 | 1.00E−08 | 459 | 1 |
| C4 | 2.1177E−10 | 3.3445E−10 | 1.5116E−10 | 2.12E−10 | 9.97E−08 | 1.00E−08 | 486 | 1 |

**Table 4** ANN-SLMB consequence of the EMMN-PPRH model for Scenario 3

| Case | MSE | | | Execution | Gradient | Mu | Epoch | Time |
|---|---|---|---|---|---|---|---|---|
| | MSE training | MSE validation | MSE testing | | | | | |
| C1 | 2.9319E−10 | 3.1247E−10 | 4.4236E−10 | 2.93E−10 | 9.99E−08 | 1.00E−08 | 670 | 2 |
| C2 | 2.3887 E−10 | 3.2580E−10 | 1.0593E−09 | 2.39E−10 | 9.97E−08 | 1.00E−08 | 542 | 2 |
| C3 | 2.0165E−10 | 4.3343E−10 | 3.9637E−10 | 2.02E−10 | 9.97E−08 | 1.00E−08 | 507 | 1 |
| C4 | 2.4663E−10 | 5.3626E−10 | 7.1892E−10 | 2.47E−10 | 9.97E−08 | 1.00E−08 | 480 | 1 |

**Table 5** ANN-SLMB consequence of the EMMN-PPRH model for Scenario 4

| Case | MSE | | | Execution | Gradient | Mu | Epoch | Time |
|---|---|---|---|---|---|---|---|---|
| | MSE training | MSE validation | MSE testing | | | | | |
| C1 | 2.1338E−10 | 3.1629E−10 | 4.0416E−10 | 2.13E−10 | 9.97E−08 | 1.00E−08 | 479 | 1 |
| C2 | 2.1338E−10 | 3.5543E−10 | 4.1233E−10 | 2.40E−10 | 9.96E−08 | 1.00E−08 | 435 | 1 |
| C3 | 1.7297E−10 | 1.6901E−10 | 7.6699E−10 | 1.73E−10 | 9.99E−08 | 1.00E−08 | 448 | 1 |
| C4 | 2.3679E−10 | 1.9375E−10 | 2.9072E−10 | 2.37E−10 | 9.96E−08 | 1.00E−08 | 430 | 1 |

**Table 6** ANN-SLMB consequence of the EMMN-PPRH model for Scenario 5

| Case | MSE | | | Execution | Gradient | Mu | Epoch | Time |
|---|---|---|---|---|---|---|---|---|
| | MSE training | MSE validation | MSE testing | | | | | |
| C1 | 1.3223E−11 | 1.5951E−11 | 1.3657E−10 | 1.32E−11 | 1.00E−07 | 1.00E−09 | 432 | 1 |
| C2 | 1.3786E−11 | 2.1300E−11 | 2.0248E−11 | 1.38E−11 | 9.98E−08 | 1.00E−09 | 444 | 1 |
| C3 | 1.0380E−11 | 1.5965E−11 | 1.1869E−11 | 1.04E−11 | 9.96E−08 | 1.00E−09 | 481 | 1 |
| C4 | 2.5603E−10 | 5.8158E−10 | 4.1644E−10 | 2.56E−10 | 9.95E−08 | 1.00E−08 | 470 | 0 |

**Table 7** ANN-SLMB consequence of the EMMN-PPRH model for Scenario 6

| Case | MSE | | | Execution | Gradient | Mu | Epoch | Time |
|---|---|---|---|---|---|---|---|---|
| | MSE training | MSE validation | MSE testing | | | | | |
| C1 | 1.1750E−11 | 3.0851E−11 | 2.3592E−11 | 1.18E−11 | 9.96E−08 | 1.00E−09 | 428 | 1 |
| C2 | 1.1815E−10 | 2.0001E−10 | 3.7015E−10 | 1.18E−10 | 9.98E−08 | 1.00E−08 | 495 | 1 |
| C3 | 1.0830E−10 | 2.0475E−10 | 1.7171E−10 | 1.08E−10 | 1.00E−07 | 1.00E−08 | 499 | 1 |
| C4 | 1.8210E−10 | 2.1362E−10 | 2.8512E−10 | 1.82E−10 | 9.97E−08 | 1.00E−08 | 475 | 1 |

and $g(\eta)$ is enumerated for the variations of rotation parameter Kr, viscosity parameter Re and electric parameter Kr in sub Fig. 12a, c, e for case 4 of scenarios 1, 2, and 3 of the EMMN-PPRH paradigm, Moreover, in sub Fig. 12b, d, f, the corresponding AE values are included in order to execute the EMMN-PPRH model technique. The impact of the rotation parameter Kr on the velocity profile is illustrated in Fig. 12a. While can be observed, as the rotation parameter rises, that increasing the motion of fluid, with the impact being more evident towards the stretching plate. Consequently, raising the rotation parameter increases the carioles force, which increases the rotational velocity and kinetic energy increases due to this rotation in fluid, which raises the motion of the flow. The electric parameter EI impacts on velocity profile is shown in Fig. 12c. It is observed that, when the values of the electric parameter increase, the velocity increases along with y and z directions, respectively. This is because a significant quantity of electric field causes rapid ionization in micro-polar nano-fluid, which causes nanoparticle motility to increase. The effect of the viscosity parameter (Re), on the velocity profile, is exposed in Fig. 12e. The velocity distribution is found to decrease as the viscosity parameter (Re) increases. This is because increasing the value of Re decreases the viscid forces that produce the well-built inertial forces, causing the velocity field to slow down.

It is feasible to see the overlapping of references and recommended solutions. As a result, for the EMMN-PPRH model, Fig. 13a, c, e demonstrate the results different magnitudes for coupling parameter $N_1$, Brownian motion parameter Nb and Prandtl number Pr for velocity $f'(\eta)$ and temperature $\theta(\eta)$ profiles for case 4 of scenarios 4, 5, and 6, respectively. Whereas in Fig. 13b, d, f the appropriate values of AE are computed. The influence of coupling parameter ($N_1$), on velocity, is indicated in Fig. 13a. It can be demonstrated that the coupling parameter ($N_1$) decreases the velocity profile towards the lower plate and raises the velocity profile from the center to the top plate. The features of the Brownian motion parameter on Temperature $\Theta(\eta)$ are depicted in Fig. 13c. The Brownian motion is the random movement of particles in nano-fluids. It is also seen that the Brownian motion of micro-polar fluid at the level of molecular is a crucial determinant in nano-fluid thermal conductivity. Growing is considered to raise the temperature profile. Furthermore, raising the Brownian motion (Nb), rises the kinetic energy of the micro polar nano-fluid within the fluid, raising the rate of heat transfer and the thickness of the boundary layer, culminating in temperature profile rises. The effect of the Prandtl number (Pr) on Temperature $\Theta(\eta)$ is presented in Fig. 13e. The temperature distribution is inversely related to Prandtl number (Pr). Temperature distribution reduces with rising Prandtl number (Pr) values and increases with decreasing Prandtl number (Pr) values. Physically, fluids with a low Prandtl number have highly thermal diffusivity, whereas fluids with a high Prandtl number Pr have the opposite effect. Because of this, a high Pr value causes the thermal boundary layer to collapse.

The results of ANN-SLMB related with HAM for all 6 scenarios, so that the absolute error was decided to approach the exactness measures from suggestion solutions, and the consequences are demonstrated in sub Figs. 12b, d, f, 13b, d, f for case 4 of scenarios 1, 2, 3, 4, 5, and 6. The AE accomplish values for scenarios 1,2,3 for velocity profiles are $10^{-07}$ to $10^{-04}$, $10^{-08}$ to $10^{-04}$ and $10^{-07}$ to $10^{-04}$ are shown in sub Fig. 12b, d, f, whereas for velocity and temperature profiles, the AE achieve values for scenarios 4, 5, and 6 are approximately $10^{-07}$ to $10^{-04}$, $10^{-08}$ to $10^{-04}$ and $10^{-08}$ to $10^{-04}$ are indicated in sub Fig. 9b, d, f, respectively. The ANN-SLMB computing methodology solves EMMN-PPRH model variations with sufficient convergent and dynamic efficiency in all of these numerical and graphical examples.

## 4 Conclusions

In this paper, the EMMN-PPRH model was analytically and numerically determined the effects of electric and magnetic fields on the micro-polar nano-fluid flow between two parallel rotating plates under the impact of Hall current.

- The solution of a mathematical model presenting EMMN-PPRH with a variation of convinced scenarios is examined by calculating an artificial neural network system using the Levenberg–Marquardt approach with backpropagation.

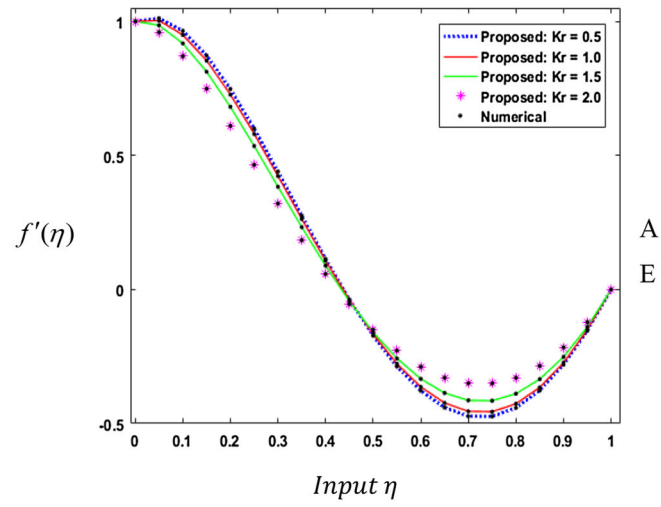


**(a)** Impact of $Kr$

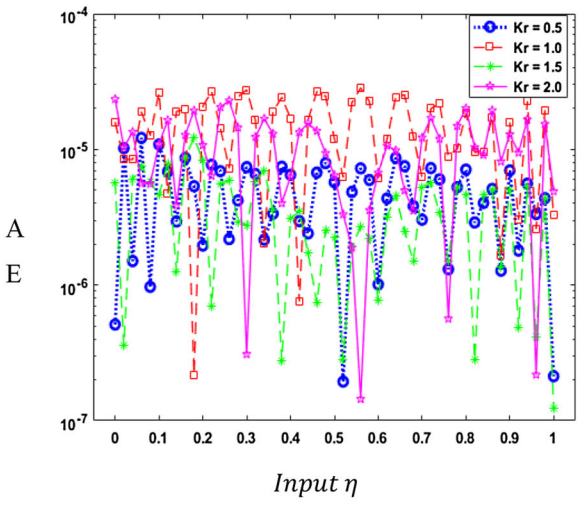


**(b)** Analysis on AE

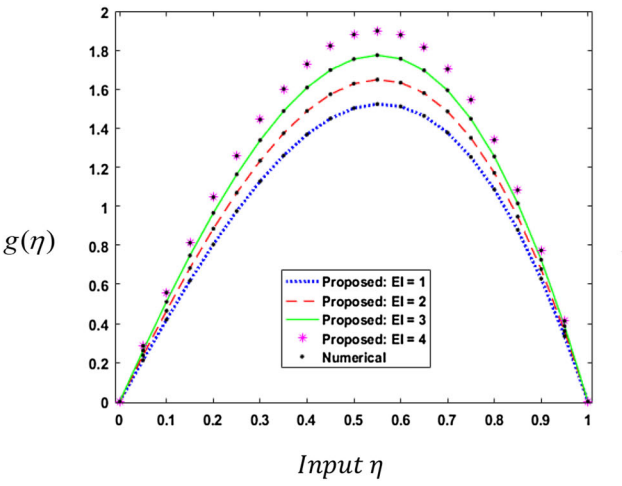


**(c)** Impact of $EI$

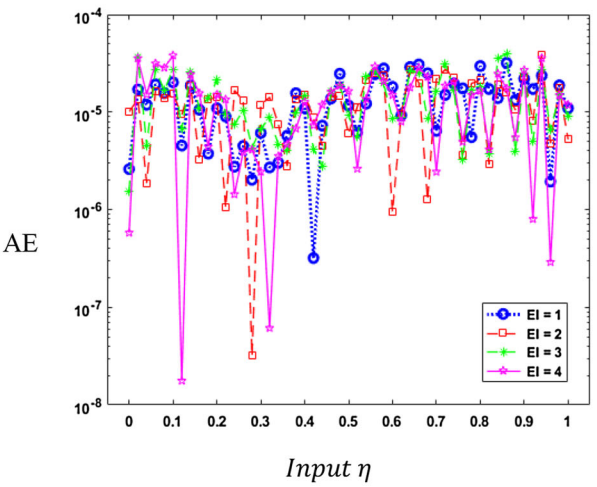


**(d)** Analysis on AE

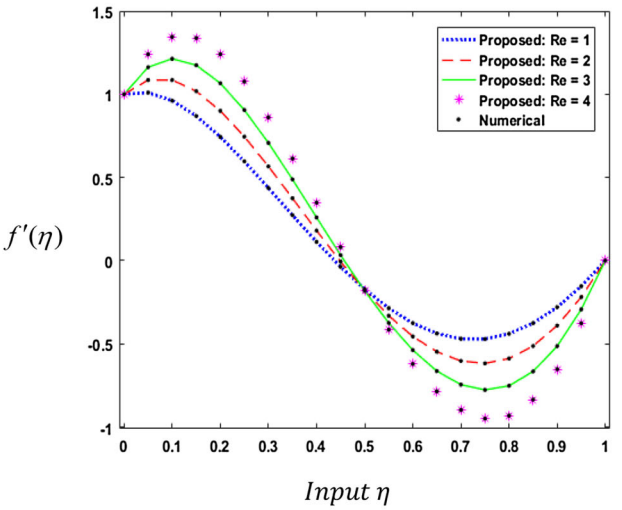


**(e)** Impact of Re

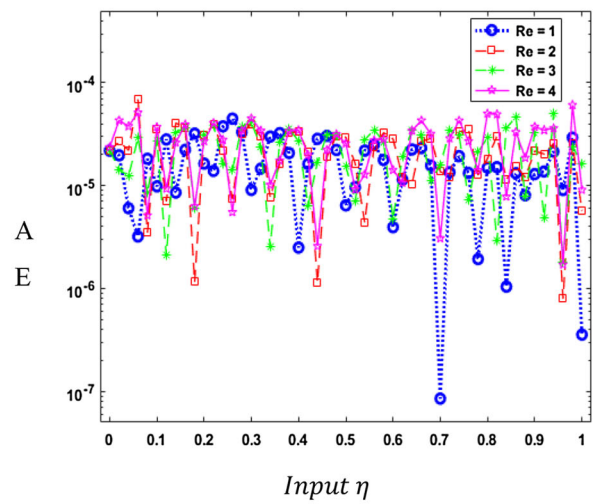


**(f)** Analysis on AE

**Fig. 12** Analysis of recommended ANN-SBLM through reference data set results for case 4 of EMMN-PPRH model scenarios 1, 2, and 3

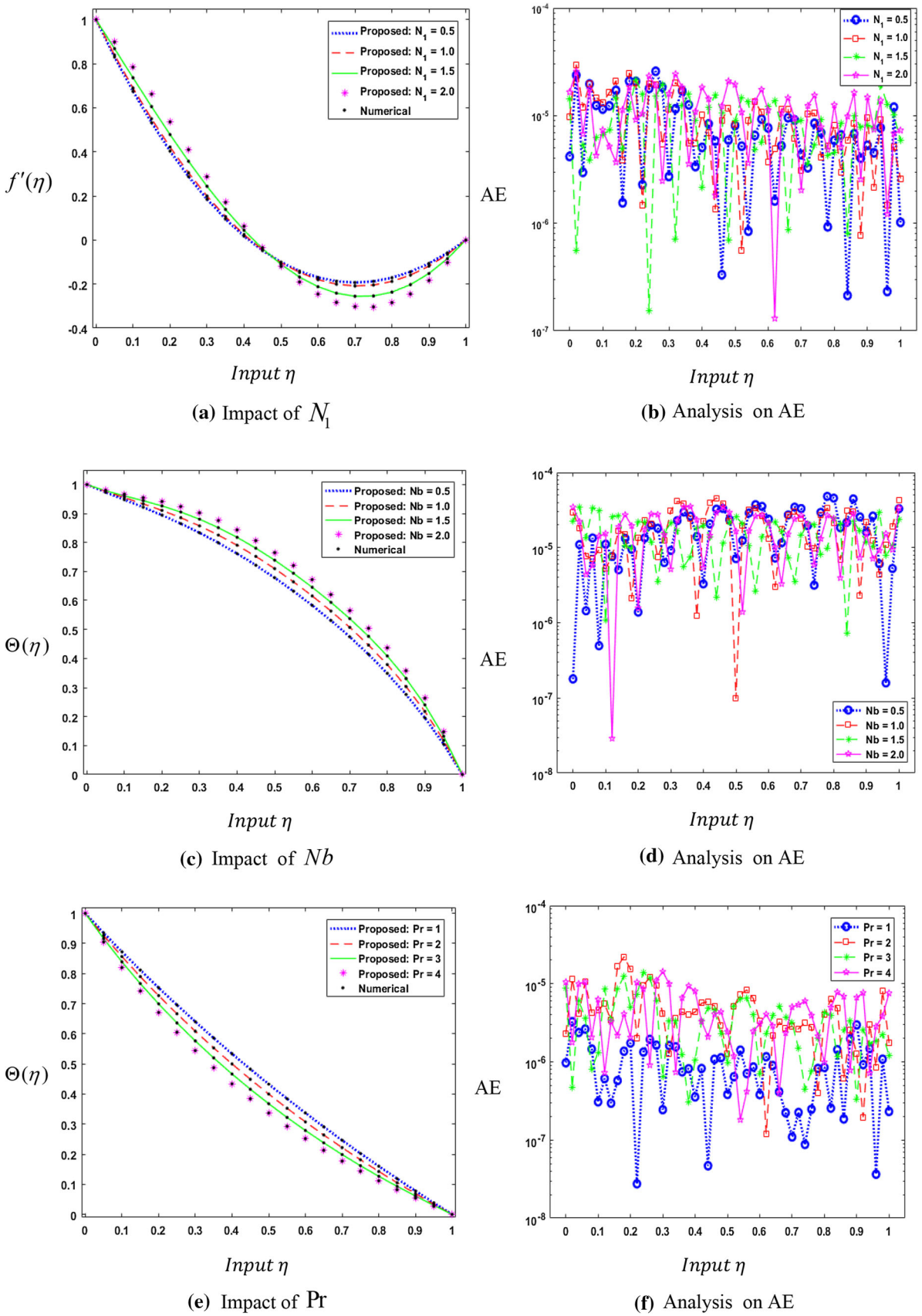


**(a)** Impact of $N_1$ **(b)** Analysis on AE

**(c)** Impact of $Nb$ **(d)** Analysis on AE

**(e)** Impact of Pr **(f)** Analysis on AE

**Fig. 13** Analysis of recommended ANN-SBLM through reference dataset results for case 4 of EMMN-PPRH model scenarios 4, 5, and 6

- The dataset for the EMMN-PPRH model is generated using the homotopy analysis analytical approach, which includes deviations from several physical measurements such as the rotation parameter, the electric parameter, the viscosity parameter, the coupling parameter, the Brownian motion parameter, and the Prandtl number.
  - In the present research, the proposed methodology ANN-SBLM based on Levenberg–Marquardt scheme is used to obtain the convergence of various parameters for velocity, temperature and concentration profiles which is closed to the solution obtain by HAM method.
  - Furthermore, we obtain some statistical data of the model that is mean square error, gradient, performance, Mu.
  - The EMMN-PPRH reference dataset is formed by modifying numerous variants, with 90%, 05%, and 05% of the dataset used for ANN-SBLM training, testing, and validation, respectively.
  - The scheme's achievement authenticates a level of $10^{-09}$ to $10^{-11}$ for both reference and recommended results, and this is further supported by graphical and numerical demonstrations of error-histogram graphs of convergence, regression dynamics, and mean square errors.

In the future, new ANN-SBLM type solvers and its hybrid versions will be designed to further investigate and address fluid mechanics challenges [77–82].

## References


1. Schmidhuber, J.: Deep Learning. Scholarpedia. **10**(11), 85–117 (2015)
2. Werbos, P.: Applications of advances in nonlinear sensitivity analysis. Syst. Model. Optim. **2**, 762–770 (1982)
3. Ahmad, I.; Ilyas, H.; Urooj, A.; Aslam, M.S.; Shoaib, M.; Raja, M.A.Z.: Novel applications of intelligent computing paradigms for the analysis of nonlinear reactive transport model of the fluid in soft tissues and microvessels. Neural Comput. Appl. **31**(12), 9041–9059 (2019)
4. Shoaib, M.; Raja, M.A.Z.; Khan, M.A.R.; Farhat, I.; Awan, S.E.: Neuro-computing networks for entropy generation under the influence of MHD and thermal radiation. Surf. Interfaces **2**, 101243 (2021)
5. Sabir, Z.; Ali, M.R.; Raja, M.A.Z.; Shoaib, M.; Núñez, R.A.S.; Sadat, R.: Computational intelligence approach using Levenberg–Marquardt backpropagation neural networks to solve the fourth-order nonlinear system of Emden-Fowler model. Eng. Comput. **3**, 1–17 (2021)
6. Uddin, I.; Ullah, I.; Raja, M.A.Z.; Shoaib, M.; Islam, S.; Muhammad, T.: Design of intelligent computing networks for numerical treatment of thin film flow of Maxwell nanofluid over a stretched and rotating surface. Surf. Interfaces **3**, 101107 (2021)
7. Khan, R.A.; Ullah, H.; Raja, M.A.Z.; Khan, M.A.R.; Islam, S.; Shoaib, M.: Heat transfer between two porous parallel plates of steady nano fludis with Brownian and Thermophoretic effects: a new stochastic numerical approach. Int. Commun. Heat Mass Transfer **126**, 105436 (2021)
8. Shah, Z.; Raja, M.A.Z.; Chu, Y.M.; Khan, W.A.; Waqas, M.; Shoaib, M.; Abbass, S.Z.: Design of neural network based intelligent computing for neumerical treatment of unsteady 3D flow of Eyring-Powell magneto-nanofluidic model. J. Market. Res. **9**(6), 14372–14387 (2020)
9. Alfvén, H.: Existence of electromagnetic-hydrodynamic waves. Nature **150**(3805), 405–406 (1942)
10. Hall, E.H.: On a new action of the magnet on electric currents. Am. J. Math. **2**(3), 287–292 (1879)
11. Ahmed, S.; Zueco, J.: Modeling of heat and mass transfer in a rotating vertical porous channel with hall current. Chem. Eng. Commun. **198**(10), 1294–1308 (2011)
12. Pop, I.; Soundalgekar, V.M.: Effects of Hall current on hydromagnetic flow near a porous plate. Acta Mech. **20**(3), 315–318 (1974)
13. Sulochana, P.: Hall effects on unsteady MHD three dimensional flow through a porous medium in a rotating parallel plate channel with effect of inclined magnetic field. Am. J. Comput. Math. **4**(05), 396 (2014)
14. Hayat, T.; Awais, M.; Nawaz, M.; Iram, S.; Alsaedi, A.: Mixed convection three-dimensional flow with Hall and ion-slip effects. Int. J. Nonlinear Sci. Numer. Simul. **14**(3–4), 167–177 (2013)
15. Abd El-Aziz, M.: Effects of Hall current on the flow and heat transfer of a nano-fluid over a stretching sheet with partial slip. Int. J. Mod. Phys. C **24**(07), 1350044 (2013)
16. Eringen, A.C.: Mechanics of micromorphic continua. In: Mechanics of Generalized Continua, pp. 18–35. Springer, Berlin (1968)
17. Eringen, A.C.: Theory of micropolar fluids. J. Math. Mech. **2**, 1–18 (1966)
18. Lukaszewicz, G.: Micropolar Fluids: Theory and Applications. Springer, Berlin (1999)
19. Mohammadein, A.A.; Gorla, R.S.R.: Effects of transverse magnetic field on mixed convection in a micropolar fluid on a horizontal plate with vectored mass transfer. Acta Mech. **118**(1), 1–12 (1996)
20. Kasiviswanathan, S.R.; Gandhi, M.V.: A class of exact solutions for the magnetohydrodynamic flow of a micropolar fluid. Int. J. Eng. Sci. **30**(4), 409–417 (1992)
21. Bhargava, R.; Kumar, L.; Takhar, H.S.: Finite element solution of mixed convection micropolar flow driven by a porous stretching sheet. Int. J. Eng. Sci. **41**(18), 2161–2178 (2003)
22. Agarwal, R.S.; Dhanapal, C.: Numerical solution of free convection micropolar fluid flow between two parallel porous vertical plates. Int. J. Eng. Sci. **26**(12), 1247–1255 (1988)
23. Srinivasacharya, D.; Murthy, J.R.; Venugopalam, D.: Unsteady stokes flow of micropolar fluid between two parallel porous plates. Int. J. Eng. Sci. **39**(14), 1557–1563 (2001)
24. Ziabakhsh, Z.; Domairry, G.: Homotopy analysis solution of micropolar flow in a porous channel with high mass transfer. Adv. Theor. Appl. Mech **1**(2), 79–94 (2008)
25. Nazar, R.; Amin, N.; Filip, D.; Pop, I.: Stagnation point flow of a micropolar fluid towards a stretching sheet. Int. J. Non-Linear Mech. **39**(7), 1227–1235 (2004)
26. Ishak, A.; Nazar, R.; Pop, I.: Magnetohydrodynamic (MHD) flow of a micropolar fluid towards a stagnation point on a vertical surface. Comput. Math. Appl. **56**(12), 3188–3194 (2008)
27. Nadeem, S.; Masood, S.; Mehmood, R.; Sadiq, M.A.: Optimal and numerical solutions for an MHD micropolar nano-fluid between rotating horizontal parallel plates. PLoS ONE **10**(6), e0124016 (2015)
28. Mehmood, R.; Nadeem, S.; Masood, S.: Effects of transverse magnetic field on a rotating micropolar fluid between parallel plates with heat transfer. J. Magn. Magn. Mater. **401**, 1006–1014 (2016)
29. Das, S.K.; Choi, S.U.; Yu, W.; Pradeep, T.: Nano-Fluids: Science and Technology. Wiley, London (2007)

30. Wang, X.Q.; Mujumdar, A.S.: A review on nano-fluids-part II: experiments and applications. Braz. J. Chem. Eng. **25**, 631–648 (2008)
31. Goodman, S.: Radiant-heat transfer between non gray parallel plates. J. Res. Natl. Bur. Stand. **58**(1), 37–40 (1957)
32. Sheikholeslami, M.; Ganji, D.D.: Three dimensional heat and mass transfer in a rotating system using nano-fluid. Powder Technol. **253**, 789–796 (2014)
33. Sheikholeslami, M.; Hatami, M.; Ganji, D.D.: Nano-fluid flow and heat transfer in a rotating system in the presence of a magnetic field. J. Mol. Liq. **190**, 112–120 (2014)
34. Attia, H.A.; Kotb, N.A.: MHD flow between two parallel plates with heat transfer. Acta Mech. **117**(1), 215–220 (1996)
35. Borkakoti, A.K.; Bharali, A.: Hydromagnetic flow and heat transfer between two horizontal plates, the lower plate being a stretching sheet. Q. Appl. Math. **40**(4), 461–467 (1983)
36. Sheikholeslami, M.: Influence of magnetic field on nano-fluid free convection in an open porous cavity by means of Lattice Boltzmann method. J. Mol. Liq. **234**, 364–374 (2017)
37. Sheikholeslami, M.: Magnetic field influence on nano-fluid thermal radiation in a cavity with tilted elliptic inner cylinder. J. Mol. Liq. **229**, 137–147 (2017)
38. Sheikholeslami, M.: Magnetohydrodynamic nano-fluid forced convection in a porous lid driven cubic cavity using Lattice Boltzmann method. J. Mol. Liq. **231**, 555–565 (2017)
39. Sheikholeslami, M.: Numerical simulation of magnetic nano-fluid natural convection in porous media. Phys. Lett. A **381**(5), 494–503 (2017)
40. Rokni, H.B.; Alsaad, D.M.; Valipour, P.: Electrohydrodynamic nano-fluid flow and heat transfer between two plates. J. Mol. Liq. **216**, 583–589 (2016)
41. Mohyud-Din, S.T.; Zaidi, Z.A.; Khan, U.; Ahmed, N.: On heat and mass transfer analysis for the flow of a nano-fluid between rotating parallel plates. Aerosp. Sci. Technol. **46**, 514–522 (2015)
42. Mahmoodi, M.; Kandelousi, S.: Application of DTM for kerosene-alumina nano-fluid flow and heat transfer between two rotating plates. The European Physical Journal Plus **130**(7), 1–11 (2015)
43. Greenspan, H.P.: The theory of rotating fluids. CUP Arch. **2**, 11158 (1968)
44. Taylor, G.I.: Experiments with rotating fluids. Proc. R. Soc. London **100**(703), 114–121 (1921)
45. Vajravelu, K.; Kumar, B.V.R.: Analytical and numerical solutions of a coupled non-linear system arising in a three-dimensional rotating flow. Int. J. Non-Linear Mech. **39**(1), 13–24 (2004)
46. Mehmood, A.; Ali, A.: Analytic solution of three-dimensional viscous flow and heat transfer over a stretching flat surface by homotopy analysis method. J. Heat Transfer **130**(12), 1158 (2008)
47. Hayat, T.; Qayyum, S.; Imtiaz, M.; Alsaedi, A.: Three-dimensional rotating flow of Jeffrey fluid for Cattaneo-Christov heat flux model. AIP Adv. **6**(2), 025012 (2016)
48. Hayat, T.; Muhammad, K.; Farooq, M.; Alsaedi, A.: Squeezed flow subject to Cattaneo-Christov heat flux and rotating frame. J. Mol. Liq. **220**, 216–222 (2016)
49. Choi, S.U. and Eastman, J.A.: Enhancing thermal conductivity of fluids with nanoparticles (No. ANL/MSD/CP-84938; CONF-951135-29). Argonne National Lab. (ANL), Argonne, IL (United States) (1995)
50. Elcock, D.: Potential impacts of nanotechnology on energy transmission applications and needs (No. ANL/EVS/TM/08-3). Argonne National Lab. (ANL), Argonne, IL (United States) (2007)
51. Liao, S.J.: Homotopy Analysis Method in Nonlinear Differential Equations. Springer, Berlin (2012)
52. Xu, D.L.; Lin, Z.L.; Liao, S.J.; Stiassnie, M.: On the steady-state fully resonant progressive waves in water of finite depth. J. Fluid Mech. **710**, 379–418 (2012)
53. Debnath, B.K.; Das, R.: Prediction of performance coefficients of a three-bucket Savonius rotor using artificial neural network. J. Renew. Sustain. Energy **2**(4), 043107 (2010)
54. Das, R.; Singh, K.; Gogoi, T.K.: Estimation of critical dimensions for a trapezoidal-shaped steel fin using hybrid differential evolution algorithm. Neural Comput. Appl. **28**(7), 1683–1693 (2017)
55. Singla, R.K.; Das, R.: A differential evolution algorithm for maximizing heat dissipation in stepped fins. Neural Comput. Appl. **30**(10), 3081–3093 (2018)
56. Das, R.; Akay, B.; Singla, R.K.; Singh, K.: Application of artificial bee colony algorithm for inverse modelling of a solar collector. Inverse Problems Sci. Eng. **25**(6), 887–908 (2017)
57. Panda, S.; Bhowmik, A.; Das, R.; Repaka, R.; Martha, S.C.: Application of homotopy analysis method and inverse solution of a rectangular wet fin. Energy Convers. Manag. **80**, 305–318 (2014)
58. Sarif, N.M.; Salleh, M.Z.; Nazar, R.: Numerical solution of flow and heat transfer over a stretching sheet with Newtonian heating using the Keller box method. Procedia Eng. **53**, 542–554 (2013)
59. Liao, S.: On the homotopy analysis method for nonlinear problems. Appl. Math. Comput. **147**(2), 499–513 (2004)
60. Wang, J.; Ye, X.: A weak Galerkin finite element method for second-order elliptic problems. J. Comput. Appl. Math. **241**, 103–115 (2013)
61. Motsa, S.S.; Dlamini, P.G.; Khumalo, M.: Spectral relaxation method and spectral quasilinearization method for solving unsteady boundary layer flow problems. Adv. Math. Phys. **2**, 1158 (2014)
62. Umar, M., et al.: A stochastic intelligent computing with neuro-evolution heuristics for nonlinear SITR system of novel COVID-19 dynamics. Symmetry **12**(10), 1628 (2020)
63. Cheema, T.N., et al.: Intelligent computing with Levenberg–Marquardt artificial neural networks for nonlinear system of COVID-19 epidemic model for future generation disease control. Eur. Phys. J. Plus **135**(11), 1–35 (2020)
64. Akbar, S., et al.: Design of bio-inspired heuristic techniques hybridized with sequential quadratic programming for joint parameters estimation of electromagnetic plane waves. Wirel. Personal Commun. **96**(1), 1475–1494 (2017)
65. Jadoon, I., et al.: Design of evolutionary optimized finite difference based numerical computing for dust density model of nonlinear van-der pol mathieu's oscillatory systems. Comput. Simul. **181**, 444–470 (2020)
66. Imran, A., et al.: Mhd and heat transfer analyses of a fluid flow through scraped surface heat exchanger by analytical solver. AIP Adv. **9**(7), 075201 (2019)
67. Raja, M.A.Z., et al.: Intelligent computing for the dynamics of entropy optimized nanofluidic system under impacts of MHD along thick surface. Int. J. Mod. Phys. B **35**(26), 2150269 (2021)
68. Ali, S., et al.: Design of evolutionary cubic spline intelligent solver for nonlinear Painlevé-I transcendent. Int. J. Modern Phys. B **2**, 2150299 (2021)
69. Jadoon, I., et al.: Integrated meta-heuristics finite difference method for the dynamics of nonlinear unipolar electrohydrodynamic pump flow model. Appl. Soft Comput. **97**, 106791 (2020)
70. Ahmad, I., et al.: Integrated neuro-evolution-based computing solver for dynamics of nonlinear corneal shape model numerically. Neural Comput. Appl. **5**, 1–17 (2020)
71. Ahmed, S.I., et al.: A new heuristic computational solver for nonlinear singular Thomas-Fermi system using evolutionary optimized cubic splines. The Eur. Phys. J. Plus **135**(1), 1–29 (2020)
72. Umar, M., et al.: A stochastic computational intelligent solver for numerical treatment of mosquito dispersal model in a heterogeneous environment. Eur. Phys. J. Plus **135**(7), 1–23 (2020)
73. Shoaib, M.; Raja, M.A.Z.; Jamshed, W.; Nisar, K.S.; Khan, I.; Farhat, I.: Intelligent computing Levenberg Marquardt approach for entropy optimized single-phase comparative study of second

grade nanofluidic system. Int. Commun. Heat Mass Transfer **127**, 105544 (2021)
74. Khan, I., et al.: Design of backpropagated intelligent networks for nonlinear second-order Lane-Emden pantograph delay differential systems. Arab. J. Sci. Eng. **2**, 1–14 (2021)
75. Sabir, Z., et al.: FMNSICS: Fractional Meyer neuro-swarm intelligent computing solver for nonlinear fractional Lane-Emden systems. Neural Comput. Appl. **3**, 1–14 (2021)
76. Sabir, Z., et al.: Integrated intelligent computing paradigm for nonlinear multi-singular third-order Emden-Fowler equation. Neural Comput. Appl. **33**(8), 3417–3436 (2021)
77. Shoaib, M.; Zubair, G.; Nisar, K.S.; Raja, M.A.Z.; Khan, M.I.; Gowda, R.P.; Prasannakumara, B.C.: Ohmic heating effects and entropy generation for nanofluidic system of Ree-Eyring fluid: Intelligent computing paradigm. Int. Commun. Heat Mass Transfer **129**, 105683 (2021)
78. Shoaib, M., et al.: A novel design of three-dimensional MHD flow of second-grade fluid past a porous plate. Math. Problems Eng. **2**, 11478 (2019)
79. Shoaib, M.; Kausar, M.; Khan, M.I.; Zeb, M.; Gowda, R.P.; Prasannakumara, B.C.; Alzahrani, F.; Raja, M.A.Z.: Intelligent backpropagated neural networks application on Darcy-Forchheimer ferrofluid slip flow system. Int. Commun. Heat Mass Transfer **129**, 105730 (2021)
80. Awan, S.E., et al.: Numerical computing paradigm for investigation of micropolar nano-fluid flow between parallel plates system with impact of electrical MHD and hall current. Arab. J. Sci. Eng. (2020). https://doi.org/10.1007/s13369-020-04736-8
81. Faisal, F.; Shoaib, M.; Raja, M.A.Z.: A new heuristic computational solver for nonlinear singular Thomas-Fermi system using evolutionary optimized cubic splines. Eur. Phys. J. Plus **135**(1), 55 (2020)
82. Aljohani, J.L.; Alaidarous, E.S.; Raja, M.A.Z.; Shoaib, M.; Alhothuali, M.S.: Intelligent computing through neural networks for numerical treatment of non-Newtonian wire coating analysis model. Sci. Rep. **11**(1), 1–32 (2021)